

Mind the Discriminability Trap in Source-Free Cross-domain Few-shot Learning

Zhenyu Zhang¹, Yixiong Zou^{1*}, Yuhua Li^{1*}, Ruixuan Li¹, Guangyao Chen²

¹ School of Computer Science and Technology, Huazhong University of Science and Technology

² National Key Laboratory for Multimedia Information Processing, Peking University

{d202481641, yixiongz, idcliyuhua, rxli}@hust.edu.cn, gy.chen@pku.edu.cn

Abstract

*Source-Free Cross-Domain Few-Shot Learning (SF-CDFSL) focuses on fine-tuning with limited training data from target domains (e.g., medical or satellite images), where Vision-Language Models (VLMs) such as CLIP and SigLIP have shown promising results. Current works in traditional visual models suggest that improving visual discriminability enhances performance. However, in VLM-based SF-CDFSL tasks, we find that **strengthening visual-modal discriminability actually suppresses VLMs’ performance**. In this paper, we aim to delve into this phenomenon for an interpretation and a solution. By both theoretical and experimental proofs, our study reveals that fine-tuning with the typical cross-entropy loss (\mathcal{L}_{vlm}) inherently includes a visual learning part and a cross-modal learning part, where the cross-modal part is crucial for rectifying the heavily disrupted modality misalignment in SF-CDFSL. However, we find that the visual learning essentially acts as a shortcut that encourages the model to reduce \mathcal{L}_{vlm} without considering the cross-modal part, therefore hindering the cross-modal alignment and harming the performance. Based on this interpretation, we further propose an approach to address this problem: first, we perturb the visual learning to guide the model to focus on the cross-modal alignment. Then, we use the visual-text semantic relationships to gradually align the visual and textual modalities during the fine-tuning. Extensive experiments on various settings, backbones (CLIP, SigLip, PE-Core), and tasks (4 CDFSL datasets and 11 FSL datasets) show that we consistently set new state-of-the-art results. Code is available at <https://github.com/zhenyuZ-HUST/CVPR26-Mind-the-Discriminability-Trap>.*

1. Introduction

Cross-domain few-shot learning (CDFSL) [14, 17, 63, 84, 86] aims to address target-domain tasks (such as medical

or satellite image recognition) with limited data by leveraging knowledge transferred from large-scale source-domain datasets (such as ImageNet). Traditional CDFSL works focus on the source-domain training to obtain a generalizable model for various target domains. However, in real-world scenarios, issues such as computational burden and data privacy make source-domain training infeasible. As a result, the source-free CDFSL task (SF-CDFSL) [46, 63, 68, 82] is proposed to focus solely on the finetuning strategy on the scarce training data of target domains. Currently, VLMs, such as CLIP [46], SigLIP [54], and PE-Core [3], have achieved promising results on in-domain few-shot learning tasks, where the classification is carried out by computing the similarity between image and text features.

In traditional visual models, it is generally believed that the more discriminative the visual features extracted by the model, the better the classification performance [33, 42, 59, 64] would be. However, in VLMs, we discover an opposite phenomenon: 1) enhancing the visual learning actually suppresses the VLMs’ performance on SF-CDFSL tasks, as in Fig. 1a (Visual learning weight > 0), and 2) **appropriately inhibiting the visual learning can achieve better fine-tuning performance on SF-CDFSL tasks**, as in Figure 1a (Visual learning weight < 0). Moreover, we also observe this phenomenon in zero-shot settings, where the best-performing CLIP model does not necessarily extract the most discriminative visual features (Fig. 1b).

In this paper, we aim to explore this phenomenon for an interpretation. Specifically, typical few-shot fine-tuning methods [24, 28, 34, 52, 71, 74] take the cross-entropy-based loss (\mathcal{L}_{vlm} , Eq. 2) between class texts and each image, which we demonstrate through mathematical derivation that involves a visual learning part and a cross-modal learning part. Recent studies [26, 27, 48, 57] indicate that in cross-domain scenarios, VLMs’ visual-text (cross-modal) alignment is heavily disrupted, making the cross-modal learning necessary in cross-domain few-shot fine-tuning. However, as both theoretically and empirically proved, we find that the visual learning actually acts as a shortcut of \mathcal{L}_{vlm} that hinders the cross-modal learning, harming the perfor-

*Corresponding author.

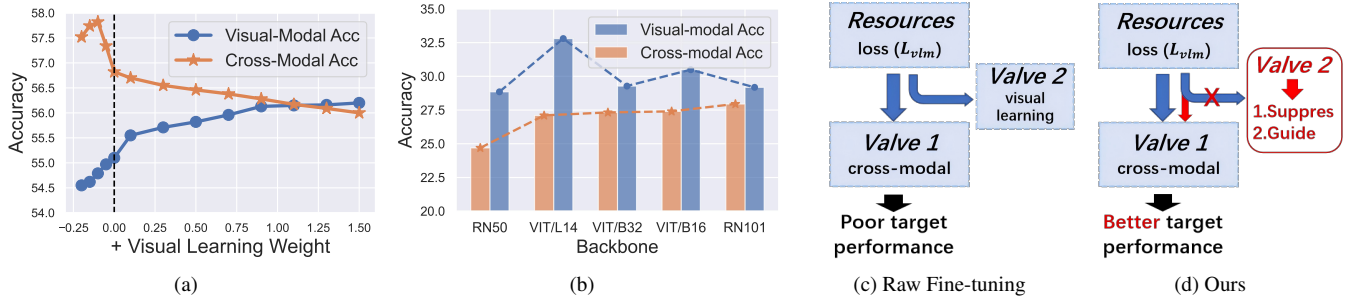


Figure 1. (a) Unlike traditional visual models, we find that enhancing visual learning consistently decreases the performance of the VLM-based CDFSL, although the visual-modal accuracy increases. Appropriately inhibiting visual learning improves cross-modal performance. (b) We also find that this phenomenon widely exists in cross-domain scenarios, where the best-performing zero-shot CLIP model does not necessarily extract the best visual features. (c) In this paper, we explore the phenomenon for an interpretation, finding that fine-tuning involves two learning directions: the visual and the cross-modal ones. We interpret visual learning as a shortcut that reduces the VLM’s classification loss but disrupts cross-modal learning. (d) Based on this, we propose a method to suppress and guide visual learning, enhancing the model’s cross-modal learning.

mance. For an intuitive understanding, we consider the fine-tuning with \mathcal{L}_{vlm} as a **two-valve bucket draining process** (Fig. 1c), where \mathcal{L}_{vlm} is the water (resources) to drain, and the visual learning and the cross-modal learning act as two valves, jointly controlling the draining process. The more resources are drained from the visual-learning-valve, the fewer resources are drained from the cross-modal-valve, therefore harming the cross-modal learning.

Based on these interpretations, we first propose the Suppressing Visual Learning (SVL) module to suppress visual learning during the fine-tuning process, guiding it to focus more on cross-modal alignment. Subsequently, we introduce the Relationship Alignment (RA) module to steer the direction of visual learning, promoting cross-modal alignment by visual-text semantic relationships. Our method is simple and effective, delivering significant performance improvements across multiple tasks with nearly zero additional overhead. Additionally, it is plug-and-play, requiring only a few lines of code to implement. Extensive experiments across various settings, backbones, and tasks demonstrate our state-of-the-art performance and generality.

In summary, we make the following contributions:

- We are the first to reveal that during the cross-entropy-based fine-tuning process, the visual learning acts as a shortcut that disrupts the important cross-modal alignment.
- We propose two simple, effective, and plug-and-play methods to constrain and correctly guide visual learning, steering the model fine-tuning process to focus on the more critical cross-modal alignment.
- We applied our methods to various VLMs and achieved significant improvements in classification performance on 4 CDFSL datasets and 11 few-shot learning datasets, achieving new state-of-the-art performance.

2. Related Work

Cross-Domain Few-Shot Learning (CDFSL) aims to train a model on a source domain that can generalize effectively to a target domain with limited examples. Existing methods are typically categorized into two types: meta-learning-based approaches [13, 17, 23, 56] and transfer learning-based approaches [17, 37, 78, 84–86]. Source-Free CDFSL (SF-CDFSL) introduces a stronger constraint by making source domain data inaccessible [63, 68, 82]. However, the influence of visual learning on VLM-based SF-CDFSL tasks remains underexplored.

In Fine-tuning, a common strategy is parameter-efficient fine-tuning (PEFT), which uses only a few samples from the target task. PEFT methods can be grouped into three main types: prompt learning [6, 28, 30, 35, 39, 66, 79–81], adapters [15, 24, 34, 52, 75], and LoRA (and its variants) [21, 71]. And, [42] use optimization-based modality inversion techniques to map representations from input modality to the complementary one.

Modality gap and misalignment is currently a key area of focus in multimodal research. [38] was the first to identify the existence of a modality gap in multimodal models. Subsequent studies [18, 26] further analyzed this gap in multimodal models. [53] pointed out a similar gap between prototypes and instances. Some research has noted that the alignment of these modalities is disrupted in cross-domain scenarios [26, 27, 48, 57]. These existing works identified the issue of modality misalignment in cross-domain scenarios and considered fine-tuning an effective method for realignment. However, our work demonstrates that fine-tuning alone is insufficient for effective realignment in cross-domain scenarios, especially for the large domain gaps in the CDFSL task, e.g., general domains vs. medical domains, which we analyze from the perspective of shortcut

learning [16, 40, 49, 70] and handle in this paper.

3. Preliminary

Source-Free Cross-Domain Few-Shot Learning: Given a target domain dataset D_T , an episode $P = \{(S, Q), Y\}$ is randomly sampled for meta-testing. This meta-testing is formulated as an N -way K -shot problem. Specifically, for each episode P_i from D_T , N classes are sampled with K labeled images to form the support set S , and the same N classes with M different images form the query set Q . The label set for these N classes is $Y = \{c_i\}_{i=1}^N$. The support set S is for training, while the query set Q is for testing.

Fine-tuning in VLMs: In classification tasks using VLMs, a textual description, known as a prompt, is generated for each class, such as “a photo of a cat”. Let r_k denote the tokenized prompt for the k -th class. The language encoder θ_t processes r_k to produce the normalized text embedding $t_k = \theta_t(r_k)$. Similarly, each image x_i is processed by the visual encoder θ_v to obtain the normalized visual embedding $f_i = \theta_v(x_i)$. The classification probability is:

$$s_{i,j} = \text{Sim}(f_i, t_j), \quad p_{i,j} = \frac{\exp(s_{i,j}/\tau)}{\sum_{j=1}^K \exp(s_{i,j}/\tau)}, \quad (1)$$

where $s_{i,j}$ represents the cosine similarity between image sample i and text prompt j , and τ is the temperature coefficient. The typical cross-entropy-based fine-tuning loss [21, 28, 71, 80] is

$$\mathcal{L}_{\text{vlm}} = -\frac{1}{N} \sum_i \log \frac{\exp(s_{i,i}/\tau)}{\sum_j \exp(s_{i,j}/\tau)}. \quad (2)$$

Visual Learning trains a classifier to perform classification [7] of visual features as follows:

$$p_{i,j} = \frac{e^{f_i w_j / \tau}}{\sum_{j=1}^K e^{f_i w_j / \tau}}, \quad \mathcal{L}_v = -\frac{1}{N} \sum_i \log \frac{e^{f_i w_i / \tau}}{\sum_{j=1}^K e^{f_i w_j / \tau}}, \quad (3)$$

where w represents the weights of the classifier. Upon completion of visual learning, the feature extractor can extract discriminative image features, and the classifier weights can be viewed as the centroid of each category.

4. Analysis of the Discriminability Trap

In VLMs, there are two types of relationships: cross-modal relationships (visual-text relationships) and intra-modal relationships (specifically, visual-modal relationships, which are the focus of this study). Among these, cross-modal relationships are more crucial as they directly determine the performance of VLMs [26, 48, 57].

During visual model classification tasks, the model is trained through visual learning (Eq. 3) to extract discriminative features. In contrast, we propose an opposite learning direction, which we call Anti-Visual Learning :

Anti-Visual Learning

We replace w in Eq. 3 with **randomly selected samples’** visual features, forming a random classifier w' . Then Anti-Visual Loss (\mathcal{L}_{ad}) is:

$$\mathcal{L}_{\text{ad}} = -\frac{1}{N} \sum_i \log \frac{e^{f_i w'_i / \tau}}{\sum_{j=1}^K e^{f_i w'_j / \tau}}. \quad (4)$$

This loss introduces perturbations, making the visual features indistinguishable and thereby suppressing visual learning.

4.1. Phenomenon

We incorporate \mathcal{L}_v and \mathcal{L}_{ad} into the fine-tuning of VLMs to control visual learning, either enhancing or inhibiting it. The results are shown in Fig. 1a. We find that visual learning (Eq. 3) improves visual-modal performance, but reduces cross-modal performance. In contrast, anti-visual learning (Eq. 4) suppresses visual-modal performance but effectively enhances cross-modal performance.

4.2. Hypothesis

4.2.1. Visual learning is part of the fine-tuning process.

To understand the reason behind this phenomenon, we first investigate the role of visual learning during the fine-tuning of VLMs. We find that during the fine-tuning process, VLM models naturally engage in visual learning:

Theorem 4.1. Let f_i and t_i represent the visual and text features of sample i , where $\|f_i\| = 1$, $\|t_i\| = 1$, and f_i^{new} represents the visual feature after gradient update. p_{ij} denotes the classification probability (Eq. 1). The difference in cosine similarity between two samples, f_i and f_k , before and after one step of training using \mathcal{L}_{vlm} (Eq. 2) is $\Delta \cos(\theta_{ik}) = f_i^{\text{new}} \cdot f_k^{\text{new}} - f_i \cdot f_k$, there is:

$$\Delta \cos(\theta_{ik}) = \eta \frac{1}{\tau} \left(f_i \cdot t_k - \sum_{j=1}^N p_{kj} f_i \cdot t_j + f_k \cdot t_i - \sum_{j=1}^N p_{ij} f_k \cdot t_j \right) + O(\eta^2), \quad (5)$$

where η is the learning rate and τ is the temperature coefficient. Detailed proof in the Appendix.

Learning objective of VLMs’ cross-entropy loss function satisfies: $f_i \cdot t_i > f_i \cdot t_j, \forall j \neq i$. Therefore: (1) When f_i and f_k belong to the same class, $t_i = t_k$, there is $\Delta \cos(\theta_{ik}) > \eta \frac{1}{\tau} (f_i \cdot t_i - 1 \cdot f_i \cdot t_i + f_k \cdot t_k - 1 \cdot f_k \cdot t_k) = 0$. (2) When f_i and f_k belong to different classes, we analyze the values of $\Delta \cos(\theta_{ik})$ during the training process across 200 episodes and observe that $\Delta \cos(\theta_{ik}) < 0$, as shown in Fig. 9. From points (1) and (2), that is, during fine-tuning, visual features of the same category cluster together while those of different categories are pushed apart, which means

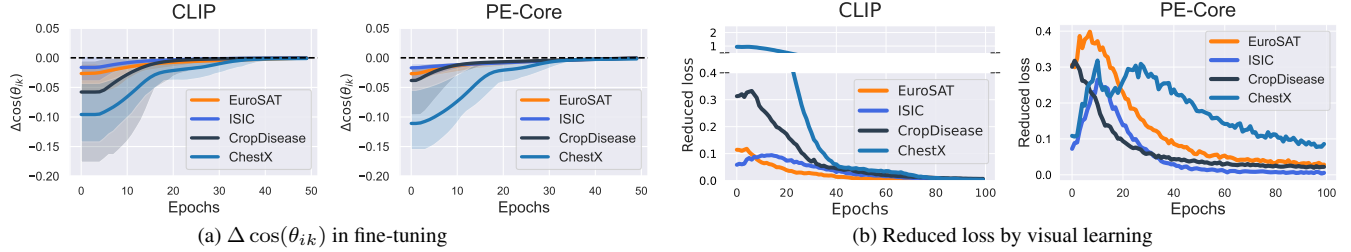


Figure 2. (a) When sample i and sample k belong to different classes, $\Delta \cos(\theta_{ik})$ in 5-way 1-shot fine-tuning is always less than 0. (b) At any stage of fine-tuning (each epoch), visual learning can effectively reduce the loss value (\mathcal{L}_{vlm}).

visual learning is consistently present in the fine-tuning process. Refer to the Appendix for detailed proof.

4.2.2. Fine-tuning is a dual-valve drainage process.

In Theorem 4.1, we demonstrated that during the fine-tuning process of VLMs based on cross-modal loss (Eq. 2), there is an inherent direction towards discriminative learning of visual features, even without explicitly guiding the model to learn such features. Therefore, fine-tuning actually drives the VLM into two learning directions: the first is the learning of cross-modal relationships, which is the primary goal of most existing VLM fine-tuning efforts [24, 34, 52, 71], while the second is visual learning, an aspect overlooked and underexplored in previous research.

With this understanding, we can visualize the VLM fine-tuning as a dual-valve drainage system (Fig. 1c). During fine-tuning, the loss value represents the resources (water) consumed, while the alignment of visual-text features (the target goal) and visual learning (the unintended goal) act as two contributing valves in this process:

Fine-tuning is a dual-valve drainage process.

Resources: Loss value (\mathcal{L}_{vlm}). The decrease in loss value during training is analogous to the drainage of resources (water) in a drainage process.

Valve1: The branch of learning of the visual-text relationship. (True target)

Valve2: The visual learning branch.

Risk: Valve 2 acts as a shortcut, reducing resource flow to Valve 1, the primary target.

Existing research [16, 49, 51] in traditional visual models suggests that such dual-branch networks have an inherent risk: **the diversion of resources will suppress the performance of the primary objective branch.** Therefore, although no prior works on VLM-based fine-tuning suggest such a risk, we hypothesize that *visual learning during the fine-tuning can also become a shortcut that diverts resources from the visual-text alignment learning, thereby harming the model’s learning of visual-text relationships.*

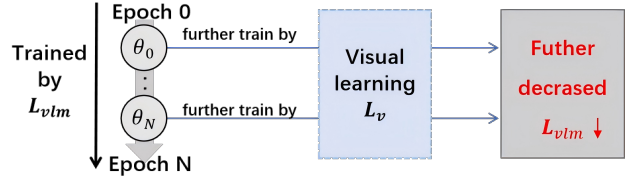


Figure 3. Recording the model at each epoch during training and further training these models using visual learning, the target loss value \mathcal{L}_{vlm} can be effectively reduced even further.

4.3. Experimental Proof

In this section, we prove our hypothesis from two aspects:

- **Visual learning can reduce the object loss.** During the fine-tuning of VLMs, visual learning can effectively reduce \mathcal{L}_{vlm} , meaning it is valve 2 that consumes resources.

- **Visual learning hinders cross-modal alignment.** Opening valve 2 (the visual learning) weakens cross-modal alignment learning, while closing it improves alignment.

4.3.1. Visual learning can reduce the object loss.

Experiment Design. The fine-tuning objective of VLM is to reduce \mathcal{L}_{vlm} (Eq. 2). To demonstrate that visual learning can also reduce \mathcal{L}_{vlm} , we save the model at each epoch during the fine-tuning process and use visual learning (Eq. 3) to further train the model (Fig. 3).

Experiment Setup. We select four CDFSL datasets [9, 20, 43, 58], and consider Vit-B/16 from CLIP [46] and PE-Core [3] as the base model, and fine-tuning by LoRA [21].

Experiment Results. We record the decrease in the loss (\mathcal{L}_{vlm}) during the visual learning. The results, shown in Fig. 2b, indicate that at each epoch of the fine-tuning process, the VLM’s loss can be reduced by visual learning that disregards the visual-text relationships. In other words, visual learning, acting as the valve 2, can consume resources and reduce the loss value.

4.3.2. Visual learning hinders cross-modal alignment.

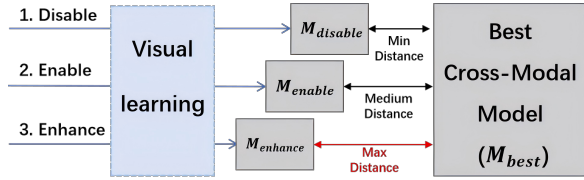


Figure 4. We employ three strategies to restrict visual learning during the VLM fine-tuning process and measure the distance of the resulting models from the optimal cross-modal model. We find that visual learning increases the distance from the optimal model, which hinders visual-text alignment.

In VLMs, cross-modal alignment is essential. One of the most direct indicators of this alignment is classification accuracy. Furthermore, we use the modality embedding shift experiment from previous work [38, 53] to measure the gap between the trained model and the optimal modality alignment model, as shown in Fig. 4. This allows us to assess the degree of modality alignment in the model.

Experiment Design. We employ three strategies: 1. Disable visual learning ($\mathcal{L}_{vlm} + \mathcal{L}_{ad}$), 2. Enable visual learning (\mathcal{L}_{vlm}), and 3. Enhance visual learning ($\mathcal{L}_{vlm} + \mathcal{L}_v$) to train and obtain models $M_{disable}$, M_{enable} , and $M_{enhance}$, respectively. We then use these models to extract text and visual features. Next, we manually adjust both the text and visual features by modifying the gap between the two sets of features, narrowing or enlarging the gap by α (Fig. 5a):

$$\vec{\Delta}_{gap} = \frac{1}{n} \sum_{i=1}^n f_i - \frac{1}{n} \sum_{i=1}^n t_i, \quad (6)$$

$$f_i^{shift} = \mathcal{N}(f_i - \alpha \vec{\Delta}_{gap}), \quad t_i^{shift} = \mathcal{N}(t_i + \alpha \vec{\Delta}_{gap}), \quad (7)$$

here, f and t represent the visual and text features, and \mathcal{N} denotes the L2 normalization operation. We then track the corresponding changes in validation loss and accuracy. If the model’s modality alignment is strong, it will exhibit high classification (as Eq. 1) accuracy and low validation loss (as Eq. 2) at its initial state. Conversely, if the alignment is weak, artificially modifying the cross-modal relationship should result in improved performance.

Experiment Setup. We select four CDFSL datasets [9, 20, 43, 58], and consider Vit-B/16 from CLIP [46] and PE-Core [3] as the base model, and fine-tuning by LoRA [21].

Experiment Results. The results are presented in Fig. 5, where the X-axis represents the modal gap, calculated as the Euclidean distance between the mean of the text features and the mean of the visual features: $\|\vec{\Delta}_{gap}\|$. The initial state of the model is indicated by the black vertical line.

Without any fine-tuning (Fig. 5b, zero shot), modality alignment is poor (the initial state does not correspond to the lowest Loss and highest Acc). However, gap shifting

can achieve higher accuracy and reduce validation loss. Using strategy 2, which fine-tunes the model without disabling visual learning (Fig. 5c), does not result in satisfactory realignment (not the lowest Loss and highest Acc). Moreover, when using strategy 3, which further enhances visual learning (Fig. 5d), the misalignment issue becomes even more pronounced (the initial state is far from the lowest Loss and highest Acc). In contrast, when we use strategy 1 to disable visual learning during the fine-tuning process (Fig. 5e), the model achieves near-optimal alignment (lowest Loss and highest Acc) without any adjustments.

To further illustrate this phenomenon, we present numerical results in Tab. 1. The metrics include classification accuracy (Acc) and the loss gap (Gap), which measures the difference between the optimal validation loss achieved via gap shifting and the initial state’s validation loss. A small loss gap indicates that the model’s initial state is nearly optimal ($M \approx M_{best}$), suggesting good modality alignment. The results (FT \rightarrow FT + \mathcal{L}_v) corroborate our findings: **visual learning hinders visual-text alignment.**

Case Study. The visualization results in Fig. 6 provide a detailed explanation of how visual learning impacts modality alignment. When visual learning is emphasized (column 2 \rightarrow column 3), the model focuses more on discriminative features. However, discriminative features alone cannot align with text such as “a photo of a Strawberry_healthy”. This reduction in attention scope hinders generalization, resulting in lower image-text similarity and poorer alignment.

4.4. Conclusion and Discussion

Based on the analysis above, we offer the following interpretation. In classification tasks on VLMs, cross-entropy loss (Eq. 2) is used as the loss function. However, during the fine-tuning process, visual learning provides a shortcut to reducing the loss function without considering cross-modal relationships, hindering the learning of the crucial cross-modal alignment.

Our insight: It is essential to appropriately constrain visual learning during the fine-tuning of the VLM model to guide the process toward prioritizing cross-modal learning.

5. Method

Based on interpretation, we further propose a method to assist the fine-tuning process of VLMs in SF-CDFSL (Fig. 7). Firstly, we propose the SVL module to suppress the model’s visual learning, encouraging the fine-tuning to prioritize the learning of cross-modal relationships. Then, we propose the RA module, using a visual-text-fused relationship matrix to guide visual-modal relationship learning, promoting alignment learning between modalities.

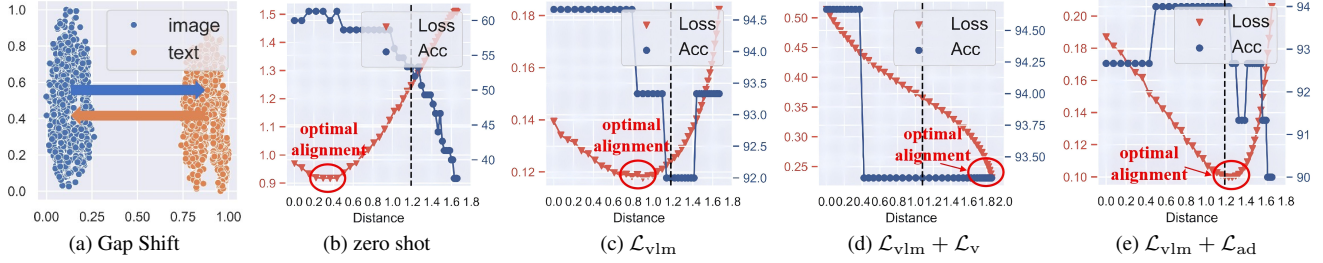


Figure 5. (a) Gap shift operation [38]. (b) The model’s initial state is marked by the vertical dashed line. In the cross-domain dataset EuroSAT, CLIP’s modalities are misaligned, meaning that through gap shift, lower loss and higher accuracy can be achieved. (c) Fine-tuning does not effectively re-align the modalities. (d) When visual learning is enhanced (\mathcal{L}_v), the misalignment becomes more pronounced. (e) When visual learning is suppressed (\mathcal{L}_{ad}), the misalignment is mitigated.

Table 1. Experiments with 800 5-way 5-shot episodes. A smaller Gap indicates better modality alignment in the model’s original state. For comparison, in *miniImageNet* [10], Acc and Gap is 98.56 / 0.007. The modality alignment is poor in cross-domain scenarios (even after fine-tuning), which is exacerbated by visual learning (\mathcal{L}_v). In contrast, our methods (\mathcal{L}_{ad} and \mathcal{L}_{ra}), enhances modality alignment.

Method	CLIP								PE-Core							
	CropDisease		EuroSAT		ISIC		ChestX		CropDisease		EuroSAT		ISIC		ChestX	
	Acc↑	Gap↓														
Fine-tune (FT, \mathcal{L}_{vlm})	95.8	0.014	93.3	0.048	52.2	0.406	24.6	0.356	97.2	0.011	94.0	0.060	59.4	0.538	24.4	0.661
FT + \mathcal{L}_v (Eq. 3)	95.6	0.022	92.7	0.072	51.9	0.626	23.2	0.742	94.2	0.118	89.0	0.211	49.4	1.312	23.0	1.752
FT + \mathcal{L}_{ad} (Eq. 4)	96.1	0.012	93.3	0.024	55.4	0.191	25.5	0.249	97.4	0.007	94.2	0.024	60.6	0.254	25.8	0.480
FT + \mathcal{L}_{ad} + \mathcal{L}_{ra}	96.6	0.009	94.2	0.027	56.1	0.171	26.6	0.238	98.1	0.005	94.8	0.022	61.4	0.193	26.8	0.438

5.1. Suppressing Visual Learning (SVL)

Let A^v denote the visual feature similarity matrix and A^t denote the text feature similarity matrix. \mathcal{F} and \mathcal{T} are the sets of visual and text features. Then, we have:

$$A^v = \mathcal{F}\mathcal{F}^T, A^t = \mathcal{T}\mathcal{T}^T. \quad (8)$$

Visual learning makes visual features of the same class similar and those of different classes distant, meaning that for any i, j where $i \neq j$, $\frac{A^v_{i,i}}{A^v_{i,j}}$ and $\frac{A^v_{j,j}}{A^v_{i,j}}$ are maximized. However, our previous analysis indicated that in VLMs, visual learning can actually harm cross-modal performance by excessively focusing on discriminative learning within the visual modality. Therefore, we propose \mathcal{L}_{ad} (Eq. 4) to suppress visual learning. Specifically, in contrast to the classifier weights that correspond one-to-one to the categories in Eq. 3, we generate classifier weights w' by using visual features of randomly selected samples from the support set and compute their cross-entropy loss, as illustrated in Fig. 7a.

5.2. Relationship Alignment (RA)

After suppressing visual learning, a further issue arises: It is necessary to provide a new direction for learning relationships within the visual modality (A^v) to facilitate cross-modal alignment. To address this, we propose using the semantics relationships extracted by the text branch (A^t) to gradually guide the learning of relationships within the visual modality, as illustrated in Fig. 7b.

Let the current epoch be e and the total number of epochs be E . Let the label list for the current batch of samples be

L . The fused relationship matrix A^{fuse} , which integrates the visual modality similarity A^v and the text modality similarity A^t , is defined as follows:

$$A^{fuse} = (1 - \frac{e}{E})A^v + \frac{e}{E}A^t[L, L]. \quad (9)$$

Here, $A^t[L, L]$ is a matrix derived by slicing A^t according to the label list L , resulting in a matrix that is the same size as A^v . Each element in this matrix, such as $(A^t[L, L])_{i,j}$, represents the similarity relationship between the classes of sample i and sample j in the text feature space, corresponding to $A^v_{i,j}$ in the visual feature space. Subsequently, A^{fuse} is used to guide the learning of relationships within the visual modality:

$$\mathcal{L}_{ra} = D_{KL}(A^v || A^{fuse}). \quad (10)$$

Here, D_{KL} represents the KL Divergence [25]. At the initial stage of training, when $e/E \approx 0$, $A^{fuse} \approx A^v$. Therefore, $\mathcal{L}_{ra} \approx D_{KL}(A^v || A^v)$, which constrains the value of A^v to remain unchanged. This has a similar effect to \mathcal{L}_{ad} : it suppresses visual learning by inhibiting changes in the relationships between visual features. As the number of training epochs increases, A^{fuse} gradually incorporates the relational information from the text features, guiding A^v to approximate the distribution of A^t . This alignment ensures that the similarity relationships between visual features become consistent with those between text features.

5.3. Two Phase Training

It is important to note that visual learning is restricted only during the early epochs of fine-tuning (see Section 6.5 for a

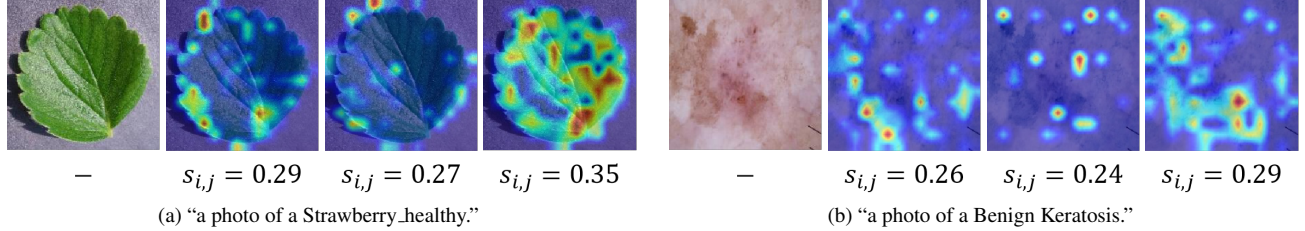


Figure 6. (a)(b) The Attention maps of the three models. From left to right: the original image, strategy 2 result (trained with \mathcal{L}_{vlm}), strategy 3 result (trained with $\mathcal{L}_{vlm} + \mathcal{L}_v$), and strategy 1 result (trained with $\mathcal{L}_{vlm} + \mathcal{L}_{ad}$). $s_{i,j}$ represents the cosine similarity between the image features and the text features. A higher similarity indicates better alignment.

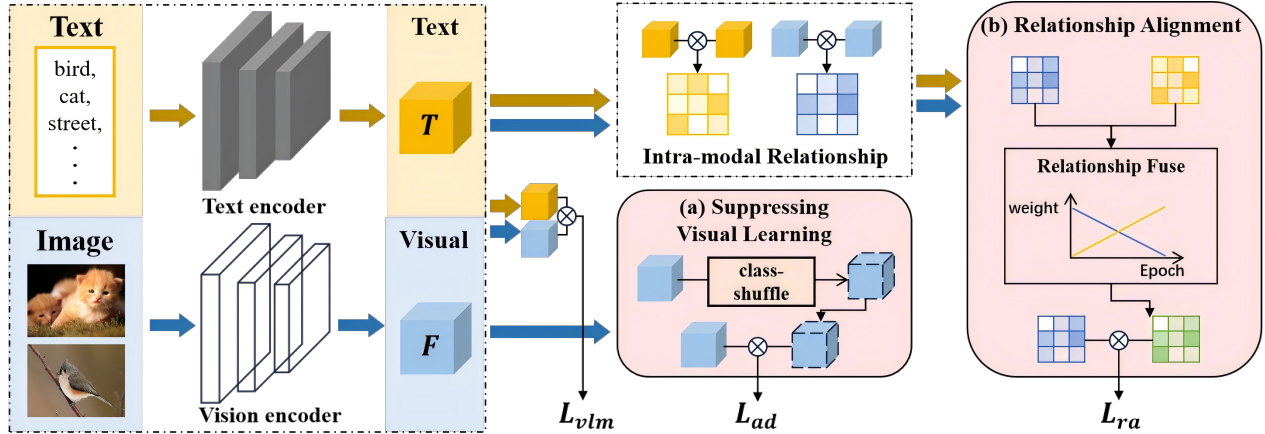


Figure 7. The overall architecture of the model, with the pink region highlighting our proposed method. (a) Firstly, we propose suppressing the visual learning to resist its shortcut during the finetuning, which constrains the model to focus more on the cross-modal alignment. (b) Then, we propose using semantic relationships to gradually align the internal relationships of the visual modality with those of the text modality, thereby enhancing cross-modal alignment.

more detailed discussion). Smaller hyperparameters, λ and β , are used to control the contributions of \mathcal{L}_{ad} and \mathcal{L}_{ra} , ensuring that the restriction on visual learning acts as a disturbance rather than dominating the entire training procedure. In subsequent epochs, we remove \mathcal{L}_{ad} and \mathcal{L}_{ra} to allow for visual learning. As a result, the fine-tuning loss function (\mathcal{L}) can be expressed as:

$$\mathcal{L} = \begin{cases} \mathcal{L}_{vlm} + \beta\mathcal{L}_{ra} + \lambda\mathcal{L}_{ad} & \text{(initial epochs)} \\ \mathcal{L}_{vlm} & \text{(later epochs)} \end{cases} \quad (11)$$

Our method can be **easily applied to any model with just a few lines of code**. See pseudocode in the Appendix.

6. Experiments

6.1. Datasets and Implementation Details

Datasets. Following previous works [46, 63, 68, 82], we do not utilize source domain datasets and finetune our model directly on the target domain. For the target domain, we utilize CropDisease [43], EuroSAT [20], ISIC [9], and ChestX [58], which are cross-domain datasets from the domains of agriculture, remote sensing, and medical data with significant domain gaps.

Implementation Details. We adopt the ViT-Base/16 network as the backbone, with parameters pre-trained by CLIP [46], SigLIP2 [54], and PE-Core [3]. We set λ to 0.1 when \mathcal{L}_{ad} is used for the visual branch (e.g., Maple, CLIP-LoRA), to 0.001 when \mathcal{L}_{ad} is used for the text branch (e.g., CoOp). We set β to 3. **See hyperparameter experiments in the Appendix.** For each episode, following [63], we perform data augmentation on the support samples. Subsequently, we train each model for 250 epochs [71], with the first 3/5 epochs (150 epochs, **see the related ablation study in the Appendix**) used as the initial training phase.

6.2. Comparison with the SOTAs

We present the performance of the most representative CDFSL task models [13, 14, 22–24, 28, 34, 52, 62, 63, 68, 71, 74, 76, 80, 84–86].

Our method, as an extension, can be applied to existing models. We selected three models that cover all possible scenarios in the fine-tuning: training only the text branch (CoOp [80]), training only the visual branch (CLIP-LoRA-Vision [71]), and training all branches (Maple [28]) to demonstrate the effectiveness of our approach.

As shown in Tab. 2, our method effectively improves per-

Table 2. Accuracies (%) of target domain datasets of 5-way 1-shot and 5-shot tasks. Refer to the Appendix for the extended table.

Task	Method	backbone	ISIC	EuroSAT	CropDisease	ChestX	Avg
5-way 1-shot	StepSTP [63]	ViT/CLIP	32.97±0.27	70.01±0.21	84.84±0.72	22.84±0.95	52.68
	Tip-Adapter [74]	ViT/CLIP	32.68±0.37	75.44±0.51	77.15±0.66	22.24±0.26	51.87
	AMU-Tuning [52]	ViT/CLIP	32.29±0.67	72.24±0.71	80.20±0.86	21.56±0.36	51.57
	LP++ [24]	ViT/CLIP	33.63±0.41	73.05±0.55	81.84±0.66	21.72±0.42	52.56
	LDC [34]	ViT/CLIP	33.72±0.46	74.39±0.52	84.07±0.61	22.32±0.36	53.62
	CoOp [80]	ViT/CLIP	32.86±0.47	72.08±0.66	80.50±0.74	21.65±0.32	51.77
	CoOp + OURS	ViT/CLIP	33.44±0.50	72.51±0.65	81.77±0.79	21.71±0.31	52.36
	Maple [28]	ViT/CLIP	33.38±0.49	76.05±0.63	81.78±0.72	21.09±0.31	53.07
	Maple + OURS	ViT/CLIP	35.11±0.51	76.92±0.65	82.51±0.69	21.64±0.34	54.05
	CLIP-LoRA-Vision [71]	ViT/CLIP	36.40±0.42	81.72±0.52	84.62±0.62	21.86±0.32	56.07
	CLIP-LoRA-Vision + OURS	ViT/CLIP	38.12±0.48	85.02±0.46	87.20±0.51	22.68±0.41	58.26
	SigLIP2-LoRA [54]	ViT/SigLip2	33.47	74.16	87.50	21.44	54.14
	SigLIP2-LoRA + OURS	ViT/SigLip2	36.88	78.04	90.85	22.27	57.01
	PE-Core-LoRA [3]	ViT/PE-Core	40.89	84.49	91.75	22.02	59.78
PE-Core-LoRA + OURS	ViT/PE-Core	45.01	86.83	93.03	23.66	62.14	
5-way 5-shot	StepSTP [63]	ViT/CLIP	52.12±0.36	89.40±1.05	96.01±0.88	26.36±0.97	65.97
	Tip-Adapter [74]	ViT/CLIP	46.96±0.59	87.24±0.33	94.19±0.39	24.07±0.44	63.12
	AMU-Tuning [52]	ViT/CLIP	44.60±0.62	88.47±0.39	94.26±0.52	23.34±0.41	62.66
	LP++ [24]	ViT/CLIP	48.49±0.44	87.48±0.42	94.47±0.38	23.89±0.29	63.58
	LDC [34]	ViT/CLIP	49.70±0.33	90.82±0.22	96.71±0.34	25.89±0.21	65.78
	CoOp [80]	ViT/CLIP	45.78±0.75	85.88±0.49	93.31±0.57	23.35±0.50	62.08
	CoOp + OURS	ViT/CLIP	45.95±0.74	86.88±0.52	93.92±0.55	23.55±0.43	62.58
	Maple [28]	ViT/CLIP	48.35±0.75	89.04±0.52	93.50±0.54	22.96±0.50	63.46
	Maple + OURS	ViT/CLIP	50.01±0.78	91.00±0.50	94.48±0.50	23.45±0.49	64.74
	CLIP-LoRA-Vision [71]	ViT/CLIP	52.22±0.71	93.31±0.47	95.88±0.42	24.61±0.47	66.50
	CLIP-LoRA-Vision + OURS	ViT/CLIP	56.14±0.46	94.14±0.34	96.64±0.39	26.61±0.43	68.38
	SigLIP2-LoRA [54]	ViT/SigLip2	51.79	91.39	96.43	24.24	65.96
	SigLIP2-LoRA + OURS	ViT/SigLip2	55.12	92.10	97.37	26.44	67.43
	PE-Core-LoRA [3]	ViT/PE-Core	58.81	94.07	97.25	24.44	68.64
PE-Core-LoRA + OURS	ViT/PE-Core	61.41	94.83	98.13	26.77	70.29	

formance across four datasets. Our method achieves new SOTA on CLIP [46], SigLIP [54], and PE-Core [3]. Also, our method can be applied to the text branch, treating each prompt as a sample. Applying our method to CoOp (CoOp + OURS) also improves its performance.

Further more, following the settings of previous works [34, 71, 81], we test our method on FSL tasks across 11 commonly used classification datasets [4, 8, 10, 12, 20, 32, 41, 44, 45, 50, 60]. As shown in Fig. 8, our method achieves optimal performance across various shot settings. Detailed results are provided in the Appendix.

6.3. Better Modality Alignment

The results in Tab 1 and 2 (higher Acc and lower Gap), Fig 5 (closer to optimal alignment), and Fig 6 (better attention scope and higher similarity) confirm that our methods enhance modality alignment. Specifically, Tab. 1 shows that adding \mathcal{L}_{ad} and \mathcal{L}_{ra} progressively improves alignment (higher Acc and lower Gap), validating the effectiveness of both modules for enhancing modality alignment.

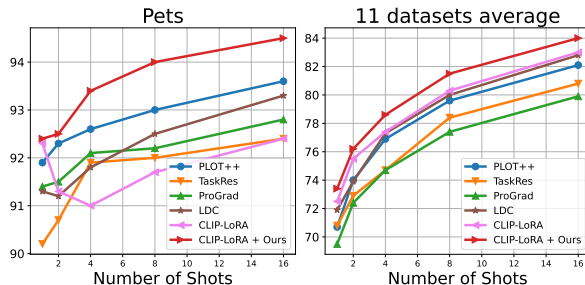


Figure 8. Average few-shot learning result of 11 datasets.

6.4. Ablation Study

We conduct ablation experiments under the 5-way 1-shot setting on four CDFSL datasets, as shown in Tab. 1 and 3. All modules in our method improve performance, with the best results achieved when all modules are used together. **Hyperparameter and alternative strategy tests for the SVL and RA modules, are in the Appendix.**

Table 3. Ablation study on 5-way 1-shot task.

SVL	RA	Cropdisease	EuroSAT	ISIC	ChestX	Avg
-	-	84.6	81.7	36.4	21.8	56.07
✓	-	86.4	83.8	37.6	22.4	57.55
-	✓	85.9	83.2	37.4	22.2	57.17
✓	✓	87.2	85.0	38.1	22.7	58.26

Table 4. Add \mathcal{L}_{ad} in different finetune phase.

Disturb Phase	Cropdisease	EuroSAT	ISIC	ChestX	Avg
No	84.62	81.72	36.40	21.86	56.07
Begin	86.40	83.82	37.62	22.38	57.55
Middle	86.02	82.77	37.36	22.04	57.04
Last	84.63	81.27	36.56	21.52	55.99
All	85.73	83.80	36.63	22.24	57.10

Table 5. Model overhead.

Method	Parameter	FLOPs	Avg Acc
CLIP-LoRA	0.884736 M	120.149333 G	56.07
CLIP-LoRA + OURS	0.884761 M	120.149359 G	58.26
Δ	$\uparrow 0.0028\%$	$\uparrow 0.000021\%$	$\uparrow 3.9\%$

6.5. When to Disturb?

In our approach, we suppress visual learning during fine-tuning using \mathcal{L}_{ad} . To find the best stage for suppression, we try to add \mathcal{L}_{ad} at different fine-tuning stages over 250 epochs: 1) **No**: don’t use \mathcal{L}_{ad} ; 2) **Begin**: the first 150 epochs (first 3/5 epochs); 3) **Middle**: 50th to 200th epochs (middle 3/5 epochs); 4) **Last**: after the 100th epoch (last 3/5 epochs); and 5) **All**: throughout the fine-tuning.

Results in Tab. 4 show **Begin** performs best, consistent with our method. The **Last** strategy performs worse than **No**, highlighting the importance of visual learning in later stages. This aligns with Fig. 2, where visual learning is strongest early in fine-tuning and should be suppressed then.

6.6. Overhead

As shown in Tab. 5, our method significantly improves performance with **virtually no additional overhead**.

7. Conclusion

In this paper, we reveal that visual learning during fine-tuning serves as a shortcut to reduce loss without considering cross-modal relationships. We then propose two methods to suppress visual learning and enhance cross-modal alignment. Extensive experiments confirm the effectiveness of our methods.

8. Acknowledgments

This work is supported by the National Key Research and Development Program of China under grant 2024YFC3307900; the National Natural Science Foundation of China under grants 62436003, 62206102, 62376103, 62302184, and 62402015; the Major Science and Technology Project of Hubei Province under grant 2025BAB011 and 2024BAA008; the Hubei Science and Technology Talent Service Project under grant 2024DJC078; Ant Group through the CCF–Ant Research Fund; the Postdoctoral Fellowship Program of the China Postdoctoral Science Foundation under grant GZB20230024; and the China Postdoctoral Science Foundation under grant 2024M750100. Computations were performed on the HPC Platform of Huazhong University of Science and Technology.

References

- [1] Shuanghao Bai, Min Zhang, Wanqi Zhou, Siteng Huang, Zhirong Luan, Donglin Wang, and Badong Chen. Prompt-based distribution alignment for unsupervised domain adaptation. In *Proceedings of the AAAI conference on artificial intelligence*, pages 729–737, 2024. 21
- [2] Jihwan Bang, Sumyeong Ahn, and Jae-Gil Lee. Active prompt learning in vision language models. In *Proceedings of the IEEE/CVF Conference on Computer Vision and Pattern Recognition*, pages 27004–27014, 2024. 15
- [3] Daniel Bolya, Po-Yao Huang, Peize Sun, Jang Hyun Cho, Andrea Madotto, Chen Wei, Tengyu Ma, Jiale Zhi, Jathushan Rajasegaran, Hanoona Rasheed, et al. Perception encoder: The best visual embeddings are not at the output of the network. *arXiv preprint arXiv:2504.13181*, 2025. 1, 4, 5, 7, 8, 17, 19, 20, 21
- [4] Lukas Bossard, Matthieu Guillaumin, and Luc Van Gool. Food-101—mining discriminative components with random forests. In *Computer vision—ECCV 2014: 13th European conference, zurich, Switzerland, September 6–12, 2014, proceedings, part VI 13*, pages 446–461. Springer, 2014. 8, 20
- [5] Arnav Chavan, Zhuang Liu, Deepak Gupta, Eric Xing, and Zhiqiang Shen. One-for-all: Generalized lora for parameter-efficient fine-tuning. *arXiv preprint arXiv:2306.07967*, 2023. 15
- [6] Guangyi Chen, Weiran Yao, Xiangchen Song, Xinyue Li, Yongming Rao, and Kun Zhang. Plot: Prompt learning with optimal transport for vision-language models. *arXiv preprint arXiv:2210.01253*, 2022. 2, 15, 20
- [7] Wei-Yu Chen, Yen-Cheng Liu, Zsolt Kira, Yu-Chiang Frank Wang, and Jia-Bin Huang. A closer look at few-shot classification. *arXiv preprint arXiv:1904.04232*, 2019. 3
- [8] Mircea Cimpoi, Subhransu Maji, Iasonas Kokkinos, Sammy Mohamed, and Andrea Vedaldi. Describing textures in the wild. In *Proceedings of the IEEE conference on computer vision and pattern recognition*, pages 3606–3613, 2014. 8, 20
- [9] Noel Codella, Veronica Rotemberg, Philipp Tschandl, M Emre Celebi, Stephen Dusza, David Gutman, Brian Helba, Aadi Kaloo, Konstantinos Liopyris, Michael Marchetti, et al. Skin lesion analysis toward melanoma detection 2018: A challenge hosted by the international skin imaging collaboration (isic). *arXiv preprint arXiv:1902.03368*, 2019. 4, 5, 7, 20
- [10] Jia Deng, Wei Dong, Richard Socher, Li-Jia Li, Kai Li, and Li Fei-Fei. Imagenet: A large-scale hierarchical image database. In *2009 IEEE conference on computer vision and pattern recognition*, pages 248–255. Ieee, 2009. 6, 8, 20
- [11] Tim Dettmers, Artidoro Pagnoni, Ari Holtzman, and Luke Zettlemoyer. Qlora: Efficient finetuning of quantized llms. *Advances in Neural Information Processing Systems*, 36, 2024. 15
- [12] Li Fei-Fei, Rob Fergus, and Pietro Perona. Learning generative visual models from few training examples: An incremental bayesian approach tested on 101 object categories. In *2004 conference on computer vision and pattern recognition workshop*, pages 178–178. IEEE, 2004. 8, 20
- [13] Yuqian Fu, Yu Xie, Yanwei Fu, Jingjing Chen, and Yu-Gang Jiang. Wave-san: Wavelet based style augmentation network for cross-domain few-shot learning. *arXiv preprint arXiv:2203.07656*, 2022. 2, 7, 15, 19, 21
- [14] Yuqian Fu, Yu Xie, Yanwei Fu, and Yu-Gang Jiang. Styleadv: Meta style adversarial training for cross-domain few-shot learning. In *Proceedings of the IEEE/CVF conference on computer vision and pattern recognition*, pages 24575–24584, 2023. 1, 7, 19, 21
- [15] Peng Gao, Shijie Geng, Renrui Zhang, Teli Ma, Rongyao Fang, Yongfeng Zhang, Hongsheng Li, and Yu Qiao. Clip-adapter: Better vision-language models with feature adapters. *International Journal of Computer Vision*, 132(2): 581–595, 2024. 2, 15
- [16] Robert Geirhos, Jörn-Henrik Jacobsen, Claudio Michaelis, Richard Zemel, Wieland Brendel, Matthias Bethge, and Felix A Wichmann. Shortcut learning in deep neural networks. *Nature Machine Intelligence*, 2(11):665–673, 2020. 3, 4
- [17] Yunhui Guo, Noel C Codella, Leonid Karlinsky, James V Codella, John R Smith, Kate Saenko, Tajana Rosing, and Rogerio Feris. A broader study of cross-domain few-shot learning. In *Computer vision—ECCV 2020: 16th European conference, glasgow, UK, August 23–28, 2020, proceedings, part XXVII 16*, pages 124–141. Springer, 2020. 1, 2, 15
- [18] Xiaoshuai Hao and Wanqian Zhang. Uncertainty-aware alignment network for cross-domain video-text retrieval. *Advances in Neural Information Processing Systems*, 36: 38284–38296, 2023. 2, 15
- [19] Masashi Hatano, Ryo Hachiuma, Ryo Fujii, and Hideo Saito. Multimodal cross-domain few-shot learning for egocentric action recognition. In *European Conference on Computer Vision (ECCV)*, 2024. 15
- [20] Patrick Helber, Benjamin Bischke, Andreas Dengel, and Damian Borth. Eurosat: A novel dataset and deep learning benchmark for land use and land cover classification. *IEEE Journal of Selected Topics in Applied Earth Observations and Remote Sensing*, 12(7):2217–2226, 2019. 4, 5, 7, 8, 20
- [21] Edward J Hu, Yelong Shen, Phillip Wallis, Zeyuan Allen-Zhu, Yuanzhi Li, Shean Wang, Lu Wang, and Weizhu Chen. Lora: Low-rank adaptation of large language models. *arXiv preprint arXiv:2106.09685*, 2021. 2, 3, 4, 5, 15
- [22] Shell Xu Hu, Da Li, Jan Stühmer, Minyoung Kim, and Timothy M Hospedales. Pushing the limits of simple pipelines for few-shot learning: External data and fine-tuning make a difference. In *Proceedings of the IEEE/CVF Conference on Computer Vision and Pattern Recognition*, pages 9068–9077, 2022. 7, 19, 21
- [23] Yanxu Hu and Andy J Ma. Adversarial feature augmentation for cross-domain few-shot classification. In *European conference on computer vision*, pages 20–37. Springer, 2022. 2, 15, 19, 21
- [24] Yunshi Huang, Fereshteh Shakeri, Jose Dolz, Malik Boudiaf, Houda Bahig, and Ismail Ben Ayed. Lp++: A surprisingly strong linear probe for few-shot clip. In *Proceedings of the IEEE/CVF Conference on Computer Vision and Pattern Recognition*, pages 23773–23782, 2024. 1, 2, 4, 7, 8, 15, 19, 21

- [25] Shuyi Ji, Zizhao Zhang, Shihui Ying, Liejun Wang, Xibin Zhao, and Yue Gao. Kullback–leibler divergence metric learning. *IEEE transactions on cybernetics*, 52(4):2047–2058, 2020. [6](#)
- [26] Zhong Ji, Zhishen Hou, Xiyao Liu, Yanwei Pang, and Jungong Han. Information symmetry matters: a modal-alternating propagation network for few-shot learning. *IEEE Transactions on Image Processing*, 31:1520–1531, 2022. [1](#), [2](#), [3](#), [15](#)
- [27] Ya Jing, Wei Wang, Liang Wang, and Tieniu Tan. Cross-modal cross-domain moment alignment network for person search. In *Proceedings of the IEEE/CVF Conference on Computer Vision and Pattern Recognition*, pages 10678–10686, 2020. [1](#), [2](#), [15](#)
- [28] Muhammad Uzair Khattak, Hanoona Rasheed, Muhammad Maaz, Salman Khan, and Fahad Shahbaz Khan. Maple: Multi-modal prompt learning. In *Proceedings of the IEEE/CVF Conference on Computer Vision and Pattern Recognition*, pages 19113–19122, 2023. [1](#), [2](#), [3](#), [7](#), [8](#), [15](#), [19](#), [20](#), [21](#)
- [29] Muhammad Uzair Khattak, Syed Talal Wasim, Muzammal Naseer, Salman Khan, Ming-Hsuan Yang, and Fahad Shahbaz Khan. Self-regulating prompts: Foundational model adaptation without forgetting. In *Proceedings of the IEEE/CVF International Conference on Computer Vision (ICCV)*, pages 15190–15200, 2023. [21](#)
- [30] Muhammad Uzair Khattak, Syed Talal Wasim, Muzammal Naseer, Salman Khan, Ming-Hsuan Yang, and Fahad Shahbaz Khan. Self-regulating prompts: Foundational model adaptation without forgetting. In *Proceedings of the IEEE/CVF International Conference on Computer Vision*, pages 15190–15200, 2023. [2](#), [15](#)
- [31] Sanghyeon Kim, Hyunmo Yang, Yunghyun Kim, Youngjoon Hong, and Eunbyung Park. Hydra: Multi-head low-rank adaptation for parameter efficient fine-tuning. *Neural Networks*, page 106414, 2024. [15](#)
- [32] Jonathan Krause, Michael Stark, Jia Deng, and Li Fei-Fei. 3d object representations for fine-grained categorization. In *Proceedings of the IEEE international conference on computer vision workshops*, pages 554–561, 2013. [8](#), [20](#)
- [33] Junnan Li, Pan Zhou, Caiming Xiong, and Steven CH Hoi. Prototypical contrastive learning of unsupervised representations. *arXiv preprint arXiv:2005.04966*, 2020. [1](#)
- [34] Shuo Li, Fang Liu, Zehua Hao, Xinyi Wang, Lingling Li, Xu Liu, Puhua Chen, and Wenping Ma. Logits deconfusion with clip for few-shot learning. In *Proceedings of the Computer Vision and Pattern Recognition Conference*, pages 25411–25421, 2025. [1](#), [2](#), [4](#), [7](#), [8](#), [15](#), [19](#), [20](#), [21](#)
- [35] Zheng Li, Xiang Li, Xinyi Fu, Xin Zhang, Weiqiang Wang, Shuo Chen, and Jian Yang. Promptkd: Unsupervised prompt distillation for vision-language models. In *Proceedings of the IEEE/CVF Conference on Computer Vision and Pattern Recognition*, pages 26617–26626, 2024. [2](#), [15](#)
- [36] Zheng Li, Yibing Song, Ming-Ming Cheng, Xiang Li, and Jian Yang. Advancing textual prompt learning with anchored attributes. In *Proceedings of the IEEE/CVF International Conference on Computer Vision*, pages 3618–3627, 2025. [15](#)
- [37] Hanwen Liang, Qiong Zhang, Peng Dai, and Juwei Lu. Boosting the generalization capability in cross-domain few-shot learning via noise-enhanced supervised autoencoder. In *Proceedings of the IEEE/CVF international conference on computer vision*, pages 9424–9434, 2021. [2](#), [15](#)
- [38] Victor Weixin Liang, Yuhui Zhang, Yongchan Kwon, Serena Yeung, and James Y Zou. Mind the gap: Understanding the modality gap in multi-modal contrastive representation learning. *Advances in Neural Information Processing Systems*, 35:17612–17625, 2022. [2](#), [5](#), [6](#), [15](#)
- [39] Zhihe Lu, Jiawang Bai, Xin Li, Zeyu Xiao, and Xinchao Wang. Beyond sole strength: Customized ensembles for generalized vision-language models. *arXiv preprint arXiv:2311.17091*, 2023. [2](#), [15](#)
- [40] Chong Ma, Lin Zhao, Yuzhong Chen, Lei Guo, Tuo Zhang, Xintao Hu, Dinggang Shen, Xi Jiang, and Tianming Liu. Rectify vit shortcut learning by visual saliency. *IEEE Transactions on Neural Networks and Learning Systems*, 2023. [3](#)
- [41] Subhransu Maji, Esa Rahtu, Juho Kannala, Matthew Blaschko, and Andrea Vedaldi. Fine-grained visual classification of aircraft. *arXiv preprint arXiv:1306.5151*, 2013. [8](#), [20](#)
- [42] Marco Mistretta, Alberto Baldrati, Lorenzo Agnolucci, Marco Bertini, and Andrew D Bagdanov. Cross the gap: Exposing the intra-modal misalignment in clip via modality inversion. *arXiv preprint arXiv:2502.04263*, 2025. [1](#), [2](#)
- [43] Sharada P Mohanty, David P Hughes, and Marcel Salathé. Using deep learning for image-based plant disease detection. *Frontiers in plant science*, 7:215232, 2016. [4](#), [5](#), [7](#), [20](#)
- [44] Maria-Elena Nilsback and Andrew Zisserman. Automated flower classification over a large number of classes. In *2008 Sixth Indian conference on computer vision, graphics & image processing*, pages 722–729. IEEE, 2008. [8](#), [20](#)
- [45] Omkar M Parkhi, Andrea Vedaldi, Andrew Zisserman, and CV Jawahar. Cats and dogs. In *2012 IEEE conference on computer vision and pattern recognition*, pages 3498–3505. IEEE, 2012. [8](#), [20](#)
- [46] Alec Radford, Jong Wook Kim, Chris Hallacy, Aditya Ramesh, Gabriel Goh, Sandhini Agarwal, Girish Sastry, Amanda Askell, Pamela Mishkin, Jack Clark, et al. Learning transferable visual models from natural language supervision. In *International conference on machine learning*, pages 8748–8763. PmlR, 2021. [1](#), [4](#), [5](#), [7](#), [8](#), [15](#), [17](#), [19](#), [20](#)
- [47] Hossein Rajabzadeh, Mojtaba Valipour, Tianshu Zhu, Marzieh Tahaei, Hyock Ju Kwon, Ali Ghodsi, Boxing Chen, and Mehdi Rezagholizadeh. Qdylora: Quantized dynamic low-rank adaptation for efficient large language model tuning. *arXiv preprint arXiv:2402.10462*, 2024. [15](#)
- [48] Zeyu Shangguan, Daniel Seita, and Mohammad Rostami. Cross-domain multi-modal few-shot object detection via rich text. In *2025 IEEE/CVF Winter Conference on Applications of Computer Vision (WACV)*, pages 6570–6580. IEEE, 2025. [1](#), [2](#), [3](#), [15](#)
- [49] Rui Song, Yingji Li, Lida Shi, Fausto Giunchiglia, and Hao Xu. Shortcut learning in in-context learning: A survey. *arXiv preprint arXiv:2411.02018*, 2024. [3](#), [4](#)

- [50] K Soomro. Ucf101: A dataset of 101 human actions classes from videos in the wild. *arXiv preprint arXiv:1212.0402*, 2012. 8, 20
- [51] Yehui Tang, Kai Han, Chang Xu, An Xiao, Yiping Deng, Chao Xu, and Yunhe Wang. Augmented shortcuts for vision transformers. *Advances in Neural Information Processing Systems*, 34:15316–15327, 2021. 4
- [52] Yuwei Tang, Zhenyi Lin, Qilong Wang, Pengfei Zhu, and Qinghua Hu. Amu-tuning: Effective logit bias for clip-based few-shot learning. In *Proceedings of the IEEE/CVF Conference on Computer Vision and Pattern Recognition*, pages 23323–23333, 2024. 1, 2, 4, 7, 8, 15, 19, 21
- [53] Hongduan Tian, Feng Liu, Zhanke Zhou, Tongliang Liu, Chengqi Zhang, and Bo Han. Mind the gap between prototypes and images in cross-domain finetuning. *Advances in Neural Information Processing Systems*, 37:11251–11289, 2025. 2, 5, 15
- [54] Michael Tschannen, Alexey Gritsenko, Xiao Wang, Muhammad Ferjad Naeem, Ibrahim Alabdulmohsin, Nikhil Parthasarathy, Talfan Evans, Lucas Beyer, Ye Xia, Basil Mustafa, et al. Siglip 2: Multilingual vision-language encoders with improved semantic understanding, localization, and dense features. *arXiv preprint arXiv:2502.14786*, 2025. 1, 7, 8, 19, 20, 21
- [55] Mojtaba Valipour, Mehdi Rezagholizadeh, Ivan Kobzyev, and Ali Ghodsi. Dylora: Parameter efficient tuning of pre-trained models using dynamic search-free low-rank adaptation. *arXiv preprint arXiv:2210.07558*, 2022. 15
- [56] Haoqing Wang and Zhi-Hong Deng. Cross-domain few-shot classification via adversarial task augmentation. *arXiv preprint arXiv:2104.14385*, 2021. 2, 15, 19, 21
- [57] Haohan Wang, Zeyi Huang, Hanlin Zhang, Yong Jae Lee, and Eric P Xing. Toward learning human-aligned cross-domain robust models by countering misaligned features. In *Uncertainty in Artificial Intelligence*, pages 2075–2084. PMLR, 2022. 1, 2, 3, 15
- [58] Xiaosong Wang, Yifan Peng, Le Lu, Zhiyong Lu, Mohammadhadi Bagheri, and Ronald M Summers. Chestx-ray8: Hospital-scale chest x-ray database and benchmarks on weakly-supervised classification and localization of common thorax diseases. In *Proceedings of the IEEE conference on computer vision and pattern recognition*, pages 2097–2106, 2017. 4, 5, 7, 20
- [59] Zhirong Wu, Yuanjun Xiong, Stella X Yu, and Dahua Lin. Unsupervised feature learning via non-parametric instance discrimination. In *Proceedings of the IEEE conference on computer vision and pattern recognition*, pages 3733–3742, 2018. 1
- [60] Jianxiong Xiao, James Hays, Krista A Ehinger, Aude Oliva, and Antonio Torralba. Sun database: Large-scale scene recognition from abbey to zoo. In *2010 IEEE computer society conference on computer vision and pattern recognition*, pages 3485–3492. IEEE, 2010. 8, 20
- [61] Zehao Xiao, Shilin Yan, Jack Hong, Jiayin Cai, Xiaolong Jiang, Yao Hu, Jiayi Shen, Qi Wang, and Cees GM Snoek. Dynaprompt: Dynamic test-time prompt tuning. In *The Thirteenth International Conference on Learning Representations*, 2025. 15
- [62] Huali Xu, Li Liu, Shuaifeng Zhi, Shaojing Fu, Zhuo Su, Ming-Ming Cheng, and Yongxiang Liu. Enhancing information maximization with distance-aware contrastive learning for source-free cross-domain few-shot learning. *IEEE Transactions on Image Processing*, 2024. 7, 19, 21
- [63] Huali Xu, Yongxiang Liu, Li Liu, Shuaifeng Zhi, Shuzhou Sun, Tianpeng Liu, and MingMing Cheng. Step-wise distribution alignment guided style prompt tuning for source-free cross-domain few-shot learning. *arXiv preprint arXiv:2411.10070*, 2024. 1, 2, 7, 8, 15, 19, 20, 21
- [64] Kaicheng Yang, Tiancheng Gu, Xiang An, Haiqiang Jiang, Xiangzi Dai, Ziyong Feng, Weidong Cai, and Jiankang Deng. Clip-cid: Efficient clip distillation via cluster-instance discrimination. In *Proceedings of the AAAI Conference on Artificial Intelligence*, pages 21974–21982, 2025. 1
- [65] Lingxiao Yang, Ru-Yuan Zhang, Yanchen Wang, and Xiaohua Xie. Mma: Multi-modal adapter for vision-language models. In *Proceedings of the IEEE/CVF Conference on Computer Vision and Pattern Recognition (CVPR)*, pages 23826–23837, 2024. 15
- [66] Hantao Yao, Rui Zhang, and Changsheng Xu. Visual-language prompt tuning with knowledge-guided context optimization. In *Proceedings of the IEEE/CVF conference on computer vision and pattern recognition*, pages 6757–6767, 2023. 2, 15, 20
- [67] Hantao Yao, Rui Zhang, and Changsheng Xu. Tcpl: Textual-based class-aware prompt tuning for visual-language model. In *Proceedings of the IEEE/CVF Conference on Computer Vision and Pattern Recognition*, pages 23438–23448, 2024. 15
- [68] Moslem Yazdanpanah and Parham Moradi. Visual domain bridge: A source-free domain adaptation for cross-domain few-shot learning. In *Proceedings of the IEEE/CVF conference on computer vision and pattern recognition*, pages 2868–2877, 2022. 1, 2, 7, 15, 19, 20, 21
- [69] Tao Yu, Zhihe Lu, Xin Jin, Zhibo Chen, and Xinchao Wang. Task residual for tuning vision-language models. In *Proceedings of the IEEE/CVF Conference on Computer Vision and Pattern Recognition*, pages 10899–10909, 2023. 20
- [70] Yu Yuan, Lili Zhao, Kai Zhang, Guangting Zheng, and Qi Liu. Do llms overcome shortcut learning? an evaluation of shortcut challenges in large language models. *arXiv preprint arXiv:2410.13343*, 2024. 3
- [71] Maxime Zanella and Ismail Ben Ayed. Low-rank few-shot adaptation of vision-language models. In *Proceedings of the IEEE/CVF Conference on Computer Vision and Pattern Recognition*, pages 1593–1603, 2024. 1, 2, 3, 4, 7, 8, 15, 19, 20, 21
- [72] Baoquan Zhang, Chuyao Luo, Demin Yu, Huiwei Lin, Xutao Li, Yunming Ye, and Bowen Zhang. Metadiff: Meta-learning with conditional diffusion for few-shot learning. In *AAAI*, 2024. 15
- [73] Qingru Zhang, Minshuo Chen, Alexander Bukharin, Nikos Karampatziakis, Pengcheng He, Yu Cheng, Weizhu Chen, and Tuo Zhao. Adalora: Adaptive budget allocation for parameter-efficient fine-tuning. *arXiv preprint arXiv:2303.10512*, 2023. 15

- [74] Renrui Zhang, Rongyao Fang, Wei Zhang, Peng Gao, Kunchang Li, Jifeng Dai, Yu Qiao, and Hongsheng Li. Tip-adapter: Training-free clip-adapter for better vision-language modeling. *arXiv preprint arXiv:2111.03930*, 2021. [1](#), [7](#), [8](#), [19](#), [21](#)
- [75] Renrui Zhang, Wei Zhang, Rongyao Fang, Peng Gao, Kunchang Li, Jifeng Dai, Yu Qiao, and Hongsheng Li. Tip-adapter: Training-free adaptation of clip for few-shot classification. In *European conference on computer vision*, pages 493–510. Springer, 2022. [2](#), [15](#), [20](#)
- [76] Yifan Zhao, Tong Zhang, Jia Li, and Yonghong Tian. Dual adaptive representation alignment for cross-domain few-shot learning. *IEEE Transactions on Pattern Analysis and Machine Intelligence*, 45(10):11720–11732, 2023. [7](#), [19](#), [21](#)
- [77] Yumiao Zhao, Bo Jiang, Yuhe Ding, Xiao Wang, Jin Tang, and Bin Luo. Fine-grained vlm fine-tuning via latent hierarchical adapter learning. *arXiv preprint arXiv:2508.11176*, 2025. [15](#)
- [78] Fei Zhou, Peng Wang, Lei Zhang, Wei Wei, and Yanning Zhang. Revisiting prototypical network for cross domain few-shot learning. In *Proceedings of the IEEE/CVF conference on computer vision and pattern recognition*, pages 20061–20070, 2023. [2](#), [15](#)
- [79] Kaiyang Zhou, Jingkang Yang, Chen Change Loy, and Ziwei Liu. Conditional prompt learning for vision-language models. In *Proceedings of the IEEE/CVF conference on computer vision and pattern recognition*, pages 16816–16825, 2022. [2](#), [15](#), [20](#)
- [80] Kaiyang Zhou, Jingkang Yang, Chen Change Loy, and Ziwei Liu. Learning to prompt for vision-language models. *International Journal of Computer Vision*, 130(9):2337–2348, 2022. [3](#), [7](#), [8](#), [15](#), [19](#), [20](#), [21](#)
- [81] Beier Zhu, Yulei Niu, Yucheng Han, Yue Wu, and Hanwang Zhang. Prompt-aligned gradient for prompt tuning. In *Proceedings of the IEEE/CVF International Conference on Computer Vision*, pages 15659–15669, 2023. [2](#), [8](#), [15](#), [20](#)
- [82] Linhai Zhuo, Zheng Wang, Yuqian Fu, and Tianwen Qian. Prompt as free lunch: Enhancing diversity in source-free cross-domain few-shot learning through semantic-guided prompting. *arXiv preprint arXiv:2412.00767*, 2024. [1](#), [2](#), [7](#), [15](#), [20](#)
- [83] Bojia Zi, Xianbiao Qi, Lingzhi Wang, Jianan Wang, Kam-Fai Wong, and Lei Zhang. Delta-lora: Fine-tuning high-rank parameters with the delta of low-rank matrices. *arXiv preprint arXiv:2309.02411*, 2023. [15](#)
- [84] Yixiong Zou, Ran Ma, Yuhua Li, and Ruixuan Li. Attention temperature matters in vit-based cross-domain few-shot learning. In *The Thirty-eighth Annual Conference on Neural Information Processing Systems*. [1](#), [2](#), [7](#), [15](#), [19](#), [21](#)
- [85] Yixiong Zou, Yicong Liu, Yiman Hu, Yuhua Li, and Ruixuan Li. Flatten long-range loss landscapes for cross-domain few-shot learning. In *Proceedings of the IEEE/CVF Conference on Computer Vision and Pattern Recognition*, pages 23575–23584, 2024. [19](#), [21](#)
- [86] Yixiong Zou, Shuai Yi, Yuhua Li, and Ruixuan Li. A closer look at the cls token for cross-domain few-shot learning. *Advances in Neural Information Processing Systems*, 37: 85523–85545, 2025. [1](#), [2](#), [7](#), [15](#), [19](#), [21](#)

Appendix

Contents

1. Introduction	1
2. Related Work	2
3. Preliminary	3
4. Analysis of the Discriminability Trap	3
4.1. Phenomenon	3
4.2. Hypothesis	3
4.2.1 . Visual learning is part of the fine-tuning process.	3
4.2.2 . Fine-tuning is a dual-valve drainage process.	4
4.3. Experimental Proof	4
4.3.1 . Visual learning can reduce the object loss.	4
4.3.2 . Visual learning hinders cross-modal alignment.	5
4.4. Conclusion and Discussion	5
5. Method	5
5.1. Suppressing Visual Learning (SVL)	6
5.2. Relationship Alignment (RA)	6
5.3. Two Phase Training	6
6. Experiments	7
6.1. Datasets and Implementation Details	7
6.2. Comparison with the SOTAs	7
6.3. Better Modality Alignment	8
6.4. Ablation Study	8
6.5. When to Disturb?	9
6.6. Overhead	9
7. Conclusion	9
8. Acknowledgments	9
A Detailed Related Work	15
A.1. Source-Free Cross-domain Few shot Learning	15
A.2. Parameter-Efficient Fine-Tuning	15
A.3. Modality Gap and Misalignment	15
B Proof of Theorem 4.1	16
C Hyperparameter Study	17
D Alternative Strategies for the SVL Module	17
E Alternative Strategies for the RA Module	18
F Division Between Initial Epochs and Later Epochs	18
G Better Modality Alignment	18
H Extended Results on CDFSL Task	19

I. Few Shot Learning Results	19
J. Datasets	20
K Implementation Details	20
L Broader Impact	20
MPseudocode	20

A. Detailed Related Work

A.1. Source-Free Cross-domain Few shot Learning

Cross-Domain Few-Shot Learning (CDFSL) aims to train a model on a source domain that can generalize effectively to a target domain with limited examples. Existing methods are typically categorized into two types: meta-learning-based approaches [13, 17, 23, 56, 72] and transfer learning-based approaches [17, 19, 37, 78, 84–86]. Source-Free Cross-Domain Few-Shot Learning (SF-CDFSL) introduces a stronger constraint by making source domain data inaccessible. Current SF-CDFSL methods [63, 68, 82] primarily rely on large models, such as CLIP [46], leveraging their prior knowledge for classification in the target domain. However, these approaches fail to account for the misalignment between modalities when transferring CLIP to cross-domain settings. Moreover, the influence of visual learning on CLIP-based SF-CDFSL tasks remains underexplored.

A.2. Parameter-Efficient Fine-Tuning

Efficiently applying Vision-Language Models (VLMs) to downstream tasks is a key research area. A common strategy is parameter-efficient fine-tuning (PEFT), which uses only a few samples from the target task. PEFT adjusts a small number of the VLM’s parameters, allowing the model to adapt to various applications without modifying all pre-trained parameters. PEFT methods can be grouped into three main types: prompt learning, adapters, and LoRA (and its variants). Prompt learning transforms fixed templates into learnable parameters, such as CoOp [80], CoCoOp [79], MaPLe [28], PLOT [6], ProGrad [81], PromptSRC [30], KgCoOp [66], PCB [2], DynaPrompt [61], TCP [67] and ATPrompt [36]. Additionally, Customized Ensemble [39] combines outputs from multiple models for improved performance, and PromptKD [35] explores knowledge distillation in prompt learning. Adapter-based methods add trainable modules to the original frozen architecture, making fine-tuning easier, such as CLIP-Adapter [15], Tip-Adapter [75], LP++ [24], AMU-Tuning [52], LatHAdapter [77], MMA [65] and LDC [34]. Low-Rank Adaptation (LoRA) [21, 71] fine-tunes the model by adding learnable low-rank matrices while keeping the original parameters fixed. The new weights can be merged with the original ones, and LoRA does not add extra inference time. Various studies have extended LoRA by adapting the rank for each matrix [55, 73], improving its performance [5, 31, 83], or reducing memory usage through quantization [11, 47]

A.3. Modality Gap and Misalignment

[38] was the first to identify the existence of a modality gap in multimodal models. Some research observed that the performance of multimodal models significantly declines when facing significant domain shifts [27, 48]. [26] highlighted the cross-modal bias between semantic-guided samples and nonsemantic-guided samples. [18] emphasized the pairwise misalignment of multimodal uncertainties, addressing the one-to-many alignment issue in multimodal video-text retrieval tasks. [53] pointed out that ProtoNet exhibits a gap between prototypes and instances in cross-domain scenarios. [57] attributed generalization errors to the model learning non-aligned features between the source domain and the test data. These existing works identified the issue of modality misalignment in cross-domain scenarios and considered fine-tuning an effective method for realignment. However, our work demonstrates that fine-tuning alone is insufficient for effective realignment in cross-domain scenarios, especially with large domain gaps in the CDFSL task, such as general domains vs. medical domains. We analyze this issue from the perspective of visual learning, which acts as a shortcut during fine-tuning, and address it in this paper.

B. Proof of Theorem 4.1

The loss in CLIP is designed to align image-text pairs while contrasting mismatched pairs. Below is the step-by-step derivation of the gradient for the visual feature f_i . For a batch of N image-text pairs, the loss for the i -th image is:

$$\mathcal{L}_i = -\log \frac{e^{f_i \cdot t_i / \tau}}{\sum_{k=1}^N e^{f_i \cdot t_k / \tau}}, \quad (12)$$

where: f_i : L2-normalized visual feature of the i -th image ($\|f_i\| = 1$). t_k : L2-normalized text feature of the k -th text ($\|t_k\| = 1$). τ : Temperature coefficient (e.g., $\tau = 0.01$).

Expand \mathcal{L}_i :

$$\begin{aligned} \mathcal{L}_i &= -\underbrace{\log \left(e^{f_i \cdot t_i / \tau} \right)}_{\text{positive}} + \underbrace{\log \left(\sum_{k=1}^N e^{f_i \cdot t_k / \tau} \right)}_{\text{negative}} \\ &= -\frac{f_i \cdot t_i}{\tau} + \log \left(\sum_{k=1}^N e^{f_i \cdot t_k / \tau} \right). \end{aligned} \quad (13)$$

The gradient $\nabla_{f_i} \mathcal{L}_i$ has two terms from the loss components:

$$\begin{aligned} \nabla_{f_i} \mathcal{L}_i &= -\nabla_{f_i} \left(\frac{f_i \cdot t_i}{\tau} \right) + \nabla_{f_i} \left(\log \left(\sum_{k=1}^N e^{f_i \cdot t_k / \tau} \right) \right) \\ &= -\frac{t_i}{\tau} + \frac{1}{\sum_{m=1}^N e^{f_i \cdot t_m / \tau}} \cdot \sum_{k=1}^N \nabla_{f_i} \left(e^{f_i \cdot t_k / \tau} \right) \\ &= -\frac{t_i}{\tau} + \frac{\sum_{k=1}^N e^{f_i \cdot t_k / \tau} \cdot \frac{t_k}{\tau}}{\sum_{m=1}^N e^{f_i \cdot t_m / \tau}} \\ &= -\frac{t_i}{\tau} + \frac{1}{\tau} \sum_{k=1}^N p_{ik} t_k \end{aligned} \quad (14)$$

where p_{ik} is the softmax probability: $p_{ik} = \frac{e^{f_i \cdot t_k / \tau}}{\sum_{m=1}^N e^{f_i \cdot t_m / \tau}}$. Let $\mathbf{f}_i^{\text{new}}$ and $\mathbf{f}_k^{\text{new}}$ represent the visual features after parameter updates. The term $\mathbf{f}_i^{\text{new}} \cdot \mathbf{f}_k^{\text{new}}$ denotes the similarity between samples i and k after the parameter update, then:

$$\mathbf{f}_i^{\text{new}} = \mathbf{f}_i + \eta \frac{1}{\tau} \left(\mathbf{t}_i - \sum_{j=1}^N p_{ij} \mathbf{t}_j \right), \quad \mathbf{f}_k^{\text{new}} = \mathbf{f}_k + \eta \frac{1}{\tau} \left(\mathbf{t}_k - \sum_{j=1}^N p_{kj} \mathbf{t}_j \right) \quad (15)$$

$$\begin{aligned} \mathbf{f}_i^{\text{new}} \cdot \mathbf{f}_k^{\text{new}} &= \left(\mathbf{f}_i + \eta \frac{1}{\tau} \left(\mathbf{t}_i - \sum_{j=1}^N p_{ij} \mathbf{t}_j \right) \right) \cdot \left(\mathbf{f}_k + \eta \frac{1}{\tau} \left(\mathbf{t}_k - \sum_{j=1}^N p_{kj} \mathbf{t}_j \right) \right) \\ &= \mathbf{f}_i \cdot \mathbf{f}_k + \eta \frac{1}{\tau} \left(\mathbf{f}_i \cdot (\mathbf{t}_k - \sum_{j=1}^N p_{kj} \mathbf{t}_j) + \mathbf{f}_k \cdot (\mathbf{t}_i - \sum_{j=1}^N p_{ij} \mathbf{t}_j) \right) + O(\eta^2), \end{aligned} \quad (16)$$

where η is the learning rate and τ is the temperature coefficient. Let the difference in cosine similarity between two samples, \mathbf{f}_i and \mathbf{f}_k , before and after one step of training is $\Delta \cos(\theta_{ik}) = \mathbf{f}_i^{\text{new}} \cdot \mathbf{f}_k^{\text{new}} - \mathbf{f}_i \cdot \mathbf{f}_k$, there is:

$$\begin{aligned} \Delta \cos(\theta_{ik}) &= \mathbf{f}_i^{\text{new}} \cdot \mathbf{f}_k^{\text{new}} - \mathbf{f}_i \cdot \mathbf{f}_k \\ &= \eta \frac{1}{\tau} \left(\mathbf{f}_i \cdot \mathbf{t}_k - \sum_{j=1}^N p_{kj} \mathbf{f}_i \cdot \mathbf{t}_j + \mathbf{f}_k \cdot \mathbf{t}_i - \sum_{j=1}^N p_{ij} \mathbf{f}_k \cdot \mathbf{t}_j \right) + O(\eta^2) \end{aligned} \quad (17)$$

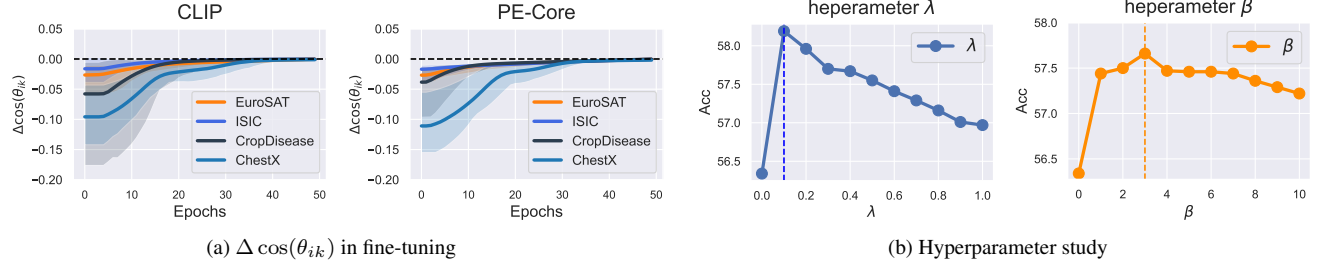


Figure 9. (a) When sample i and sample k belong to different classes, $\Delta \cos(\theta_{ik})$ in 5-way 1-shot fine-tuning is always less than 0, which means that the visual features of samples i and k from different classes will become increasingly dissimilar. (b) Hyperparameter study.

When \mathbf{f}_i and \mathbf{f}_k belong to the same class, $\mathbf{t}_i = \mathbf{t}_k$. Considering that the learning objective of the cross-entropy loss function satisfies: $\mathbf{f}_i \cdot \mathbf{t}_i > \mathbf{f}_i \cdot \mathbf{t}_j, \forall j \neq i$. there is:

$$\begin{aligned}
 \Delta \cos(\theta_{ik}) &= \eta \frac{1}{\tau} \left(\mathbf{f}_i \cdot \mathbf{t}_i - \sum_{j=1}^N p_{kj} \mathbf{f}_i \cdot \mathbf{t}_j + \mathbf{f}_k \cdot \mathbf{t}_k - \sum_{j=1}^N p_{ij} \mathbf{f}_k \cdot \mathbf{t}_j \right) + O(\eta^2) \\
 &> \eta \frac{1}{\tau} \left(\mathbf{f}_i \cdot \mathbf{t}_i - \left(\sum_{j=1}^N p_{kj} \right) \mathbf{f}_i \cdot \mathbf{t}_i + \mathbf{f}_k \cdot \mathbf{t}_k - \left(\sum_{j=1}^N p_{ij} \right) \mathbf{f}_k \cdot \mathbf{t}_k \right) \\
 &= \eta \frac{1}{\tau} (\mathbf{f}_i \cdot \mathbf{t}_i - 1 \cdot \mathbf{f}_i \cdot \mathbf{t}_i + \mathbf{f}_k \cdot \mathbf{t}_k - 1 \cdot \mathbf{f}_k \cdot \mathbf{t}_k) = 0.
 \end{aligned} \tag{18}$$

That is, the visual features between samples i and k of the same class will become increasingly similar.

When \mathbf{f}_i and \mathbf{f}_k belong to different classes, we analyzed the values of $\Delta \cos(\theta_{ik})$ during the training process across 200 episodes, as shown in Figure 9. As seen, in different VLMs (CLIP [46] and PE-Core [3]), the $\Delta \cos(\theta_{ik})$ is always less than 0., which means that the visual features of samples i and k from different classes will become increasingly dissimilar.

Summary: during fine-tuning, visual features of the same category cluster together while those of different categories are pushed apart, which means visual learning is consistently present in the fine-tuning process.

C. Hyperparameter Study

Our method involves two main hyperparameters: λ , corresponding to the Suppressing Visual Learning (SVL) module, and β , corresponding to the Relationship Alignment (RA) module. Here, we present the 5-way 1-shot performance corresponding to different values of λ and β on the four CDFSL datasets, as shown in Figure 9b. As observed, the model achieves peak performance when λ is set to 0.1 and β to 3. A smaller value for λ is preferred, as \mathcal{L}_{ad} functions as a perturbation and should be assigned a small weight to prevent it from dominating the training process.

D. Alternative Strategies for the SVL Module

In this section, we discuss several alternative strategies for the SVL modules. The SVL module is designed to perturb the visual learning, thereby guiding the model to focus more on learning cross-modal relationships. Our approach involves randomly sampling support samples to create class-shuffle weights and performing the classification task on the visual branch (as described in Section 5.1 of the main text). To demonstrate the effectiveness of this strategy, we also test three other approaches: **NO**, which does not use the SVL module and serves as the baseline, and $-\mathcal{L}_v$, which use the negative of \mathcal{L}_v as \mathcal{L}_{ad} , where $\mathcal{L}_{ad} = -\mathcal{L}_v$ (as defined in Equation 3 of the paper). Additionally, **Noise Proto** generates class-shuffle weights using random initialization (non-true visual features) and then performs the classification task on the visual branch.

Table 6. Alternative strategies for the SVL module.

Disturb Strategy	Cropdisease	EuroSAT	ISIC	ChestX	Avg
No	84.62	81.72	36.40	21.86	56.07
$-\mathcal{L}_v$	82.41	78.84	34.72	21.37	54.33
Noise Proto	84.31	82.42	35.96	21.80	56.12
Ours	86.41	83.80	37.63	22.38	57.55

Table 7. Alternative strategies for the RA module.

Alignment Strategy	Cropdisease	EuroSAT	ISIC	ChestX	Avg
No	84.62	81.72	36.40	21.86	56.07
only vision	84.87	82.61	36.94	22.11	56.63
only text	84.14	81.36	36.87	21.34	55.92
Ours	85.92	83.21	37.42	22.17	57.17

The results, shown in Table 6, indicate that the $-\mathcal{L}_v$ strategy actually harms the model’s performance. Moreover, the **Noise Proto** strategy brings little or no improvement in performance. This is understandable, as a fundamental requirement for visual learning is that the learning occurs within a valid visual feature distribution. The class-shuffle weights generated by the **Noise Proto** strategy may not be within this valid distribution. In contrast, our approach ensures the simulation of an effective visual feature distribution while simultaneously suppressing discriminative learning, leading to a significant improvement in model performance.

E. Alternative Strategies for the RA Module

In this section, we discuss several alternative strategies for the RA modules. The RA module is designed to replace the discriminative visual feature learning direction in the fine-tuning process, providing a new learning direction that facilitates alignment between modalities. Our approach promotes cross-modal alignment by gradually aligning the internal relationships of visual features with those of textual features (as described in Section 5.2 of the main text). To demonstrate the effectiveness of this strategy, we also test three other approaches: **NO**, which does not use the RA module and serves as the baseline, and **only vision**, which does not incorporate the internal relationships of the text modality and only maintains the relationships between visual features, i.e., $\mathcal{L}_{ra} = D_{KL}(A^v||A^v)$ (see Equation 10 in the main text). Additionally, **only text** does not use the gradual fusion approach (Equation 9 in the main text) but directly aligns the internal relationships of visual features with those of textual features, i.e., $\mathcal{L}_{ra} = D_{KL}(A^v||A^t)$.

The results, shown in Table 7, indicate that the **only text** strategy harms the model’s performance. In contrast, our method, which gradually fuses the relationships between visual features A_v and textual features A_t to guide the learning of internal visual feature relationships, most effectively promotes alignment between modalities and achieves optimal performance.

F. Division Between Initial Epochs and Later Epochs

During the fine-tuning process, we train the model for 250 epochs, with the first 3/5 epochs used as the initial training phase. In this section, we conduct further experiments and analysis on the initial training phase. We test different proportions for the initial training phase division, as shown in Figure 10. The results indicate that when 150 epochs (the first 3/5) is used as the initial training phase, the model achieves optimal performance across four datasets. It is important to note that in this section, we focus only on using the initial epochs for the initial training phase, as Section 6.5 of the main text has already demonstrated the need to suppress visual learning in the early stages.

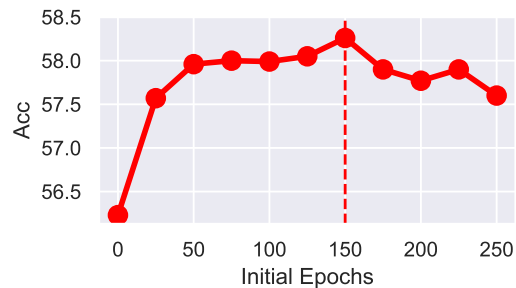


Figure 10. Results for different initial epochs settings.

G. Better Modality Alignment

Additionally, the modules we proposed effectively facilitate the cross-modal alignment process. Firstly, as shown in Table 1, both of our proposed modules improves cross-modal classification performance while reducing the loss gap, indicating that models fine-tuned with our approach achieve good modality alignment. Secondly, as illustrated in Figure 6 and Figure 11, our method enables the model to focus on the appropriate scope. In the baseline model, due to its strong visual learning, it tends to focus on the most discriminative small features in the image (second column), which is detrimental to modality alignment. In this case, the visual features are dominated by a small, discriminative part of the image. For example, in the case of ”a photo of a Strawberry_healthy,” the most discriminative feature of the strawberry leaf is its serrated edges, but this feature

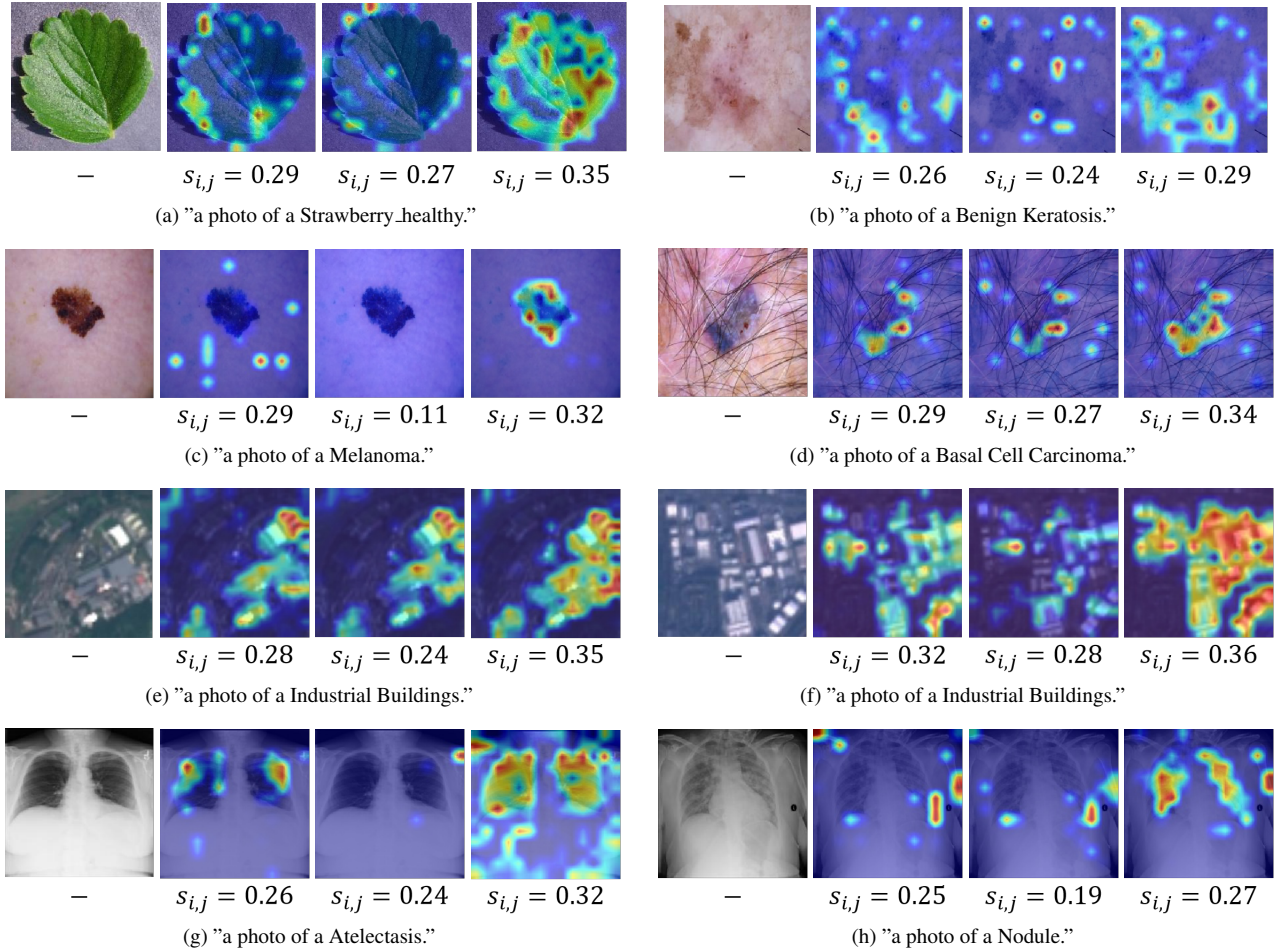


Figure 11. The attention maps of the three models are shown. From left to right: the original image, the Baseline result (trained with \mathcal{L}_{vlm}), the result of the model with enhanced visual learning (trained with $\mathcal{L}_{vlm} + \mathcal{L}_v$), and the result of our method (trained with $\mathcal{L}_{vlm} + \mathcal{L}_{ad}$). Here, $s_{i,j}$ represents the cosine similarity between the image features and the text features. A higher similarity indicates better alignment. It is evident that our model has the most appropriate attention scope and achieves the highest similarity between sample pairs.

alone cannot fully represent the semantic information of "strawberry leaf." Our method, by suppressing this visual learning, leads to a more generalized model. As seen in the fourth column, after applying our method, the model is able to focus correctly on the image features corresponding to the semantic information. This promotes cross-modal alignment, resulting in a significantly higher similarity between the image and text features.

H. Extended Results on CDFSL Task

Table 8 is an extended version of Table 2 in the main text. It includes the performance of various models on four CDFSL datasets under different settings. These settings involve different backbones (CLIP [46], SigLIP2 [54], and PE-Core [3]), the use of a source dataset (Source), and whether fine-tuning on the target domain is applied (FT). Specifically, the methods include ATA [56], AFA [23], wave-SAN [13], StyleAdv [14], StyleAdv-FT (fine-tuned StyleAdv), DARA [76], PMF [22], FLOR [85], CD-CLS [86], AttnTemp [84], VDB [68], IM-DCL [62], StepSTP [63], CoOp [80], Tip-Adapter [74], AMU-Tuning [52], LP++ [24], LDC [34], Maple [28], and CLIP-LoRA [71], which are introduced as our competitors.

I. Few Shot Learning Results

We further evaluate the effectiveness of our method on 11 commonly used classification datasets. Following the setup of previous work [71, 80], we evaluate our approach on 11 datasets covering various fine-grained classification tasks: scenes

(SUN397 [60]), aircraft types (Aircraft [41]), satellite imagery (EuroSAT [20]), automobiles (StanfordCars [32]), food items (Food101 [4]), pet breeds (OxfordPets [45]), flowers (Flower102 [44]), general objects (Caltech101 [12]), textures (DTD [8]), and human actions (UCF101 [50]), in addition to ImageNet [10]. These datasets provide a comprehensive benchmarking framework for evaluating few-shot visual classification tasks.

We compare our model against several prompt-based methods, including CoOp [80] with 4 learnable tokens, CoOp [80] with 16 learnable tokens, CoCoOp [79], PLOT++ [6] (an adaptation of the original PLOT designed for transformer architectures), KgCoOp [66], MaPLe [28], and ProGrad [81] with 16 tokens. Additionally, we evaluate adapter-based methods such as Tip-Adapter-F [75] and TaskRes [69] and LDC [34], as well as the LoRA-based method CLIP-LoRA [71]. These comparative methods provide a comprehensive benchmark to assess the effectiveness of our proposed approach in few-shot visual classification tasks.

Our method is plug-and-play, allowing for quick integration into existing approaches. As shown in Table 9, applying our method to the existing CLIP-LoRA [71] model effectively enhances its few-shot classification performance across 11 datasets. In addition, it achieves the highest average classification accuracy under various shot settings.

J. Datasets

Following previous works [46, 63, 68, 82], we do not utilize source domain datasets and finetune our model directly on the target domain. For the target domain we utilize CropDisease [43], EuroSAT [20], ISIC [9], and ChestX [58], which are cross-domain datasets from the domain of agriculture, remote sensing, and medical data with significant domain gaps.

K. Implementation Details

In the experiments, we adopt the ViT-Base/16 network as the primary feature extraction network, with parameters pre-trained by CLIP [46], SigLIP2 [54] and PE-Core [3]. For the parameter λ , we consider two cases: when \mathcal{L}_{ad} is used for the visual branch (e.g., Maple, CLIP-LoRA), λ is set to 0.1; when used for the text branch (e.g., CoOp), λ is set to 0.001. The parameter β is set to 0.5 in all cases. For each episode, following [63], we first perform data augmentation on the support samples. Subsequently, for each method, we train for 250 epochs, and the first 150 epochs are used as the initial epochs, employing \mathcal{L}_{ad} and \mathcal{L}_{ra} . We evaluate every network using 15 query samples per class, randomly selecting 800 tasks, and report the average results (%) with the 95% confidence interval. We use an NVIDIA GeForce RTX 3090 GPU for training and testing.

L. Broader Impact

In this paper, we observe the misalignment of modalities in CLIP under cross-domain scenarios and reveal that the cross-entropy-based fine-tuning process inherently incorporates strong visual learning. This learning direction acts as a shortcut, allowing the model to reduce the loss without considering cross-modal relationships, leading to suppression of cross-modal relationship learning. Based on these findings, We then propose two methods to suppress visual learning and enhance cross-modal alignment. Our research is crucial for future studies on fine-tuning VLM models in cross-domain scenarios. It highlights the impact of visual learning on fine-tuning, a factor that has been overlooked in previous work. While our method has been evaluated across four distinct target domains, offering a promising initial assessment of its cross-domain applicability, the diversity of these domains may not fully capture all potential real-world scenarios. Future work will focus on expanding our evaluations to include a broader range of target domains to better understand the method’s performance in diverse real-world contexts.

M. Pseudocode

Below is the pseudocode for fine-tuning the model in a few-shot learning setting. The parts highlighted in red correspond to the implementation of our method. Our method can be implemented with just a few lines of code.

Table 8. The accuracy(%) of four target domain datasets under 5-way 1-shot and 5-way 5-shot tasks. The use of a source dataset (Source), and whether fine-tuning on the target domain is applied (FT)

Task	Method	backbone	Source	FT	ISIC	EuroSAT	CropDisease	ChestX	Avg
5-way 1-shot	ATA [56]	RN10	Y	-	33.21±0.40	61.35±0.50	67.47±0.50	22.10±0.20	46.03
	AFA [23]	RN10	Y	-	33.21±0.30	63.12±0.50	67.61±0.50	22.92±0.20	46.72
	wave-SAN [13]	RN10	Y	-	33.35±0.71	69.64±1.09	70.80±1.06	22.93±0.49	49.18
	StyleAdv [14]	RN10	Y	-	33.96±0.57	70.94±0.82	74.13±0.78	22.64±0.35	50.42
	ATA-FT [56]	RN10	Y	Y	34.94±0.40	68.62±0.50	75.41±0.50	22.15±0.20	50.28
	DARA [76]	RN10	Y	Y	36.42±0.64	67.42±0.80	80.74±0.76	22.92±0.40	51.88
	StyleAdv-FT [14]	RN10	Y	Y	35.76±0.52	72.92±0.75	80.69±0.28	22.64±0.35	53.00
	PMF [22]	ViT/DINO	Y	Y	30.36±0.36	70.74±0.63	80.79±0.62	21.73±0.30	50.91
	StyleAdv-FT [14]	ViT/DINO	Y	Y	33.99±0.46	74.93±0.58	84.11±0.57	22.92±0.32	53.99
	FLoR [85]	ViT/DINO	Y	Y	35.49	73.09	83.55	23.26	53.85
	CD-CLS [86]	ViT/DINO	Y	Y	35.56	74.97	84.53	23.39	54.62
	AttnTemp [84]	ViT/DINO	Y	Y	38.05	75.09	84.78	23.63	55.39
	FN+VDB [68]	RN18	-	Y	32.96±0.57	69.67±0.80	79.68±0.74	22.64±0.41	51.24
	IM-DCL [62]	RN10	-	Y	38.13±0.57	77.14±0.71	84.37±0.99	23.98±0.79	55.91
	StepSTP [63]	ViT/CLIP	-	Y	32.97±0.27	70.01±0.21	84.84±0.72	22.84±0.95	52.68
	CoOp [80]	ViT/CLIP	-	Y	32.86±0.47	72.08±0.66	80.50±0.74	21.65±0.32	51.77
	Tip-Adapter [74]	ViT/CLIP	-	Y	32.68±0.37	75.44±0.51	77.15±0.66	22.24±0.26	51.87
	PromptSRC [29]	ViT/CLIP	-	Y	31.86±0.57	73.44±0.71	76.15±0.89	21.16±0.36	50.65
	PDA [1]	ViT/CLIP	-	Y	31.45±0.44	69.68±0.71	79.20±0.83	20.66±0.28	50.25
	AMU-Tuning [52]	ViT/CLIP	-	Y	32.29±0.67	72.24±0.71	80.20±0.86	21.56±0.36	51.57
	LP++ [24]	ViT/CLIP	-	Y	33.63±0.41	73.05±0.55	81.84±0.66	21.72±0.42	52.56
	LDC [34]	ViT/CLIP	-	Y	33.72±0.46	74.39±0.52	84.07±0.61	22.32±0.36	53.62
	Maple [28]	ViT/CLIP	-	Y	33.38±0.49	76.05±0.63	81.78±0.72	21.09±0.31	53.07
	Maple + OURS	ViT/CLIP	-	Y	35.11±0.51	76.92±0.65	82.51±0.69	21.64±0.34	54.05
	CLIP-LoRA-Vision [71]	ViT/CLIP	-	Y	36.40±0.42	81.72±0.52	84.62±0.62	21.86±0.32	56.07
	CLIP-LoRA-Vision + OURS	ViT/CLIP	-	Y	38.12±0.48	85.02±0.46	87.20±0.51	22.68±0.41	58.26
	SigLIP2-LoRA [54]	ViT/SigLip2	-	Y	33.47	74.16	87.50	21.44	54.14
	SigLIP2-LoRA + OURS	ViT/SigLip2	-	Y	36.88	78.04	90.85	22.27	57.01
	PE-Core-LoRA [3]	ViT/PE-Core	-	Y	40.89	84.49	91.75	22.02	59.78
	PE-Core-LoRA + OURS	ViT/PE-Core	-	Y	45.01	86.83	93.03	23.66	62.14
5-way 5-shot	ATA [56]	RN10	Y	-	44.91±0.40	83.75±0.40	90.59±0.30	24.32±0.40	60.89
	AFA [23]	RN10	Y	-	46.01±0.40	85.58±0.40	88.06±0.30	25.02±0.20	61.17
	wave-SAN [13]	RN10	Y	-	44.93±0.67	85.22±0.71	89.70±0.64	25.63±0.49	61.37
	StyleAdv [14]	RN10	Y	-	45.77±0.51	86.58±0.54	93.65±0.39	26.07±0.37	63.02
	ATA-FT [56]	RN10	Y	Y	49.79±0.40	89.64±0.30	95.44±0.20	25.08±0.20	64.99
	DARA [76]	RN10	Y	Y	56.28±0.66	85.84±0.54	95.32±0.34	27.54±0.42	66.25
	StyleAdv-FT [14]	RN10	Y	Y	53.05±0.54	91.64±0.43	96.51±0.28	26.24±0.35	66.86
	PMF [22]	ViT/DINO	Y	Y	50.12	85.98	92.96	27.27	64.08
	StyleAdv-FT [14]	ViT/DINO	Y	Y	51.23±0.51	90.12±0.33	95.99±0.27	26.97±0.33	66.08
	FLoR [85]	ViT/DINO	Y	Y	53.06	90.75	96.47	27.02	66.83
	CD-CLS [86]	ViT/DINO	Y	Y	54.69	91.53	96.27	27.66	67.54
	AttnTemp [84]	ViT/DINO	Y	Y	54.91	90.82	96.66	28.03	67.61
	FN+VDB [68]	RN18	-	Y	47.48±0.59	87.31±0.50	94.63±0.37	25.55±0.43	64.74
	IM-DCL [62]	RN10	-	Y	52.74±0.69	89.47±0.42	95.73±0.38	28.93±0.41	66.72
	StepSTP [63]	ViT/CLIP	-	Y	52.12±0.36	89.40±1.05	96.01±0.88	26.36±0.97	65.97
	CoOp [80]	ViT/CLIP	-	Y	45.78±0.75	85.88±0.49	93.31±0.57	23.35±0.50	62.08
	Tip-Adapter [74]	ViT/CLIP	-	Y	46.96±0.59	87.24±0.33	94.19±0.39	24.07±0.44	63.12
	PromptSRC [29]	ViT/CLIP	-	Y	46.09±0.48	86.54±0.49	89.97±0.41	23.51±0.47	61.52
	PDA [1]	ViT/CLIP	-	Y	45.19±0.62	86.21±0.44	92.67±0.39	21.87±0.33	61.48
	AMU-Tuning [52]	ViT/CLIP	-	Y	44.60±0.62	88.47±0.39	94.26±0.52	23.34±0.41	62.66
	LP++ [24]	ViT/CLIP	-	Y	48.49±0.44	87.48±0.42	94.47±0.38	23.89±0.29	63.58
	LDC [34]	ViT/CLIP	-	Y	49.70±0.33	90.82±0.22	96.71±0.34	25.89±0.21	65.78
	Maple [28]	ViT/CLIP	-	Y	48.35±0.75	89.04±0.52	93.50±0.54	22.96±0.50	63.46
	Maple + OURS	ViT/CLIP	-	Y	50.01±0.78	91.00±0.50	94.48±0.50	23.45±0.49	64.74
	CLIP-LoRA-Vision [71]	ViT/CLIP	-	Y	52.22±0.71	93.31±0.47	95.88±0.42	24.61±0.47	66.50
	CLIP-LoRA-Vision + OURS	ViT/CLIP	-	Y	56.14±0.46	94.14±0.34	96.64±0.39	26.61±0.43	68.38
	SigLIP2-LoRA [54]	ViT/SigLip2	-	Y	51.79	91.39	96.43	24.24	65.96
	SigLIP2-LoRA + OURS	ViT/SigLip2	-	Y	55.12	92.10	97.37	26.44	67.43
	PE-Core-LoRA [3]	ViT/PE-Core	-	Y	58.81	94.07	97.25	24.44	68.64
	PE-Core-LoRA + OURS	ViT/PE-Core	-	Y	61.41	94.83	98.13	26.77	70.29

Table 9. Detailed results for 11 datasets using ViT-B/16 as the visual backbone are presented. Top-1 accuracy, averaged over 3 random seeds, is reported. The highest value is highlighted in bold, and the second-highest performance is underlined.

Shots	Method	ImageNet	SUN	Aircraft	EuroSAT	Cars	Food	Pets	Flowers	Caltech	DTD	UCF	Average
1	CoOp(4)	68.0	67.3	26.2	50.9	67.1	82.6	90.3	72.7	93.2	50.1	70.7	67.2
	CoOp(16)	65.7	67.0	20.8	56.4	67.5	84.3	90.2	78.3	92.5	50.1	71.2	67.6
	CoCoOp	69.4	68.7	28.1	55.4	67.6	84.9	91.9	73.4	94.1	52.6	70.4	68.8
	TIP-Adapter-F	69.4	67.2	28.8	67.8	67.1	85.8	90.6	83.8	94.0	51.6	73.4	70.9
	CLIP-Adapter	67.9	65.4	25.2	49.3	65.7	86.1	89.0	71.3	92.0	44.2	66.9	65.7
	PLOT++	66.5	66.8	28.6	65.4	68.8	86.2	91.9	80.5	94.3	54.6	74.3	70.7
	KgCoOp	68.9	68.4	26.8	61.9	66.7	86.4	92.1	74.7	94.2	52.7	72.8	69.6
	TaskRes	69.6	68.1	31.3	65.4	68.8	84.6	90.2	81.7	93.6	53.8	71.7	70.8
	MaPLe	69.7	69.3	28.1	29.1	67.6	85.4	91.4	74.9	93.6	50.0	71.1	66.4
	ProGrad	67.0	67.0	28.8	57.0	68.2	84.9	91.4	80.9	93.5	52.8	73.3	69.5
	LDC	69.5	68.0	27.5	78.4	68.2	85.8	91.3	83.6	93.8	58.2	73.2	72.5
	CLIP-LoRA	70.4	70.4	30.2	72.3	70.1	84.3	92.3	83.2	93.7	54.3	76.3	72.5
CLIP-LoRA + Ours	70.4	70.7	30.9	78.4	70.7	86.5	92.4	83.9	93.9	<u>54.8</u>	76.4	73.5	
2	CoOp(4)	68.7	68.0	28.1	66.2	70.5	82.6	89.9	80.9	93.0	53.7	73.5	70.5
	CoOp(16)	67.0	67.0	25.9	65.1	70.4	84.4	89.9	88.0	93.1	54.1	74.1	70.8
	CoCoOp	70.1	69.4	29.3	61.8	68.4	85.9	91.9	77.8	94.4	52.3	73.4	70.4
	TIP-Adapter-F	70.0	68.6	32.8	73.2	70.8	86.0	91.6	90.1	93.9	57.8	76.2	73.7
	CLIP-Adapter	68.2	67.2	27.0	51.2	66.6	86.2	89.7	71.7	93.4	45.4	68.4	66.8
	PLOT++	68.3	68.1	31.1	76.8	73.2	86.3	92.3	89.8	94.7	56.7	76.8	74.0
	KgCoOp	69.6	69.6	28.0	69.2	68.2	86.6	92.3	79.8	94.5	55.3	74.6	71.6
	TaskRes	70.2	70.5	32.7	70.2	72.1	85.6	90.7	84.4	94.3	55.6	75.2	72.9
	MaPLe	70.0	70.7	29.5	59.4	68.5	86.5	91.8	79.8	94.9	50.6	74.0	70.5
	ProGrad	69.1	69.0	31.1	66.3	72.4	84.8	91.5	87.5	93.6	56.0	75.6	72.4
	LDC	69.8	69.6	30.0	81.7	70.75	86.1	91.2	88.7	94.3	62.2	75.9	74.5
	CLIP-LoRA	70.8	71.3	33.2	82.7	73.2	83.2	91.3	89.8	94.6	59.9	80.0	75.5
CLIP-LoRA + Ours	70.8	72.3	33.4	83.1	73.5	86.6	92.5	90.4	<u>94.7</u>	<u>60.8</u>	<u>79.5</u>	76.2	
4	CoOp(4)	69.7	70.6	29.7	65.8	73.4	83.5	92.3	86.6	94.5	58.5	78.1	73.0
	CoOp(16)	68.8	69.7	30.9	69.7	74.4	84.5	92.5	92.2	94.5	59.5	77.6	74.0
	CoCoOp	70.6	70.4	30.6	61.7	69.5	86.3	92.7	81.5	94.8	55.7	75.3	71.7
	TIP-Adapter-F	70.7	70.8	35.7	76.8	74.1	86.5	91.9	92.1	94.8	59.8	78.1	75.6
	CLIP-Adapter	68.6	68.0	27.9	51.2	67.5	86.5	90.8	73.1	94.0	46.1	70.6	67.7
	PLOT++	70.4	71.7	35.3	83.2	76.3	86.5	92.6	92.9	95.1	62.4	79.8	76.9
	KgCoOp	69.9	71.5	32.2	71.8	69.5	86.9	92.6	87.0	95.0	58.7	77.6	73.9
	TaskRes	71.0	72.7	33.4	74.2	76.0	86.0	91.9	85.0	95.0	60.1	76.2	74.7
	MaPLe	70.6	71.4	30.1	69.9	70.1	86.7	93.3	84.9	95.0	59.0	77.1	73.5
	ProGrad	70.2	71.7	34.1	69.6	75.0	85.4	92.1	91.1	94.4	59.7	77.9	74.7
	LDC	71.0	72.9	31.9	86.3	75.1	86.7	91.8	93.9	95.2	66.4	79.7	77.3
	CLIP-LoRA	71.4	72.8	37.9	84.9	77.4	82.7	91.0	93.7	95.2	<u>63.8</u>	81.1	77.4
CLIP-LoRA + Ours	71.4	73.7	39.2	86.4	78.0	87.0	93.4	94.3	95.8	<u>65.2</u>	81.3	78.7	
8	CoOp(4)	70.8	72.4	37.0	74.7	76.8	83.3	92.1	95.0	94.7	63.7	79.8	76.4
	CoOp(16)	70.6	71.9	38.5	77.1	79.0	82.7	91.3	94.9	94.5	64.8	80.0	76.8
	CoCoOp	70.8	71.5	32.4	69.1	70.4	87.0	93.3	86.3	94.9	60.1	75.9	73.8
	TIP-Adapter-F	71.7	73.5	39.5	81.3	78.3	86.9	91.8	94.3	95.2	66.7	82.0	78.3
	CLIP-Adapter	69.1	71.7	30.5	61.6	70.7	86.9	91.9	83.3	94.5	50.5	76.2	71.5
	PLOT++	71.3	73.9	41.4	88.4	81.3	86.6	93.0	95.4	95.5	66.5	82.8	79.6
	KgCoOp	70.2	72.6	34.8	73.9	72.8	87.0	93.0	91.5	95.1	65.6	80.0	76.0
	TaskRes	72.3	74.6	40.3	77.5	79.6	86.4	92.0	96.0	95.3	66.7	81.6	78.4
	MaPLe	71.3	73.2	33.8	82.8	71.3	87.2	93.1	90.5	95.1	63.0	79.5	76.4
	ProGrad	71.3	73.0	37.7	77.8	78.7	86.1	92.2	95.0	94.8	63.9	80.5	77.4
	LDC	72.4	75.5	38.0	90.8	79.7	86.9	92.5	96.0	95.9	71.5	80.9	80.0
	CLIP-LoRA	72.3	74.7	45.7	89.7	82.1	83.1	91.7	96.3	95.6	67.5	84.1	80.3
CLIP-LoRA + Ours	72.4	75.5	48.6	90.9	82.5	87.3	94.0	96.9	95.9	<u>69.5</u>	84.1	81.6	
16	CoOp(4)	71.5	74.6	40.1	83.5	79.1	85.1	92.4	96.4	95.5	69.2	81.9	79.0
	CoOp(16)	71.9	74.9	43.2	85.0	82.9	84.2	92.0	96.8	95.8	69.7	83.1	80.0
	CoCoOp	71.1	72.6	33.3	73.6	72.3	87.4	93.4	89.1	95.1	63.7	77.2	75.4
	TIP-Adapter-F	73.4	76.0	44.6	85.9	82.3	86.8	92.6	96.2	95.7	70.8	83.9	80.7
	CLIP-Adapter	69.8	74.2	34.2	71.4	74.0	87.1	92.3	92.9	94.9	59.4	80.2	75.5
	PLOT++	72.6	76.0	46.7	92.0	84.6	87.1	93.6	97.6	96.0	71.4	85.3	82.1
	KgCoOp	70.4	73.3	36.5	76.2	74.8	87.2	93.2	93.4	95.2	68.7	81.7	77.3
	TaskRes	73.0	76.1	44.9	82.7	83.5	86.9	92.4	97.5	95.8	71.5	84.0	80.8
	MaPLe	71.9	74.5	36.8	87.5	74.3	87.4	93.2	94.2	95.4	68.4	81.4	78.6
	ProGrad	72.1	75.1	43.0	83.6	82.9	85.8	92.8	96.6	95.9	68.8	82.7	79.9
	LDC	73.8	76.9	47.8	92.1	84.1	87.3	93.3	97.8	96.4	77.0	84.4	82.8
	CLIP-LoRA	73.6	76.1	54.7	92.1	86.3	84.2	92.4	98.0	96.4	72.0	86.7	83.0
CLIP-LoRA + Ours	73.4	76.9	57.3	92.5	86.6	87.7	94.5	98.4	96.5	<u>73.2</u>	<u>86.1</u>	84.0	

Algorithm 1 Suppressing Visual Learning and Relationship Alignment

Require: Pretrained VLMs with visual encoder θ_v and text encoder θ_t , tokenized prompts for all classes $\{r_k\}$, few-shot labeled samples $\{(\mathbf{x}_i, y_i)\}$, and hyperparameters λ and β .

- 1: **for** each labeled sample (\mathbf{x}_i, y_i) **do**
 - 2: Obtain visual feature $f_i = \theta_v(\mathbf{x}_i)$
 - 3: **end for**
 - 4: **for** each prompt $r_j \in \{r_k\}$ **do**
 - 5: Obtain text feature $t_j = \theta_t(r_j)$
 - 6: **end for**
 - 7: Compute logits $\mathcal{S} = \mathcal{F}\mathcal{T}^T$.
 - 8: Using \mathcal{S} to compute cross-entropy loss \mathcal{L}_{vlm} .
 - 9: Compute visual feature similarity matrix $A^v = \mathcal{F}\mathcal{F}^T$.
 - 10: Compute text feature similarity matrix $A^t = \mathcal{T}\mathcal{T}^T$.
 - 11: Randomly generate index I_{rand} .
 - 12: Compute class-shuffle logits as $\mathcal{S}_{\text{rand}} = A^v[:, I_{\text{rand}}]$.
 - 13: Using $\mathcal{S}_{\text{rand}}$ as new logits to compute cross-entropy loss as the anti-visual loss \mathcal{L}_{ad} .
 - 14: Fusing A^v and A^t to get A^{fuse} .
 - 15: Compute relationship alignment loss \mathcal{L}_{ra} .
 - 16: Total loss $\mathcal{L} = \mathcal{L}_{\text{vlm}} + \beta\mathcal{L}_{\text{ra}} + \lambda\mathcal{L}_{\text{ad}}$.
-